JOURNAL OF PETROLOGY

Journal of Petrology, 2019, Vol. 60, No. 2, 269–300
doi: 10.1093/petrology/egy114
Advance Access Publication Date: 19 December 2018
Original Article

OXFORD

Droplets and Bubbles: Solidification of Sulphide-rich Vapour-saturated Orthocumulates in the Norilsk-Talnakh Ni–Cu–PGE Ore-bearing Intrusions

Stephen J. Barnes [1]*, Margaux Le Vaillant[1], Belinda Godel[1] and C. Michael Lesher[2]

[1]CSIRO Mineral Resources, PO Box 1130 Bentley, WA 6102, Australia; [2]Laurentian University, Sudbury, Canada

*Corresponding author. CSIRO Mineral Resources, Kensington, WA, Australia.
E-mail: Steve.barnes@csiro.au

Received July 30, 2018; Accepted November 30, 2018

ABSTRACT

A common feature of the mineralised chonolith intrusions of the Norilsk-Talnakh camp is the presence of globular disseminated Ni–Cu–Fe sulphide ores, particularly well developed within the olivine orthocumulate layers of the intrusions, locally referred to as picritic gabbrodolerites. In many cases these globules partially fill subspherical intercumulus spaces within a framework of crystals of olivine and/or plagioclase. The sulphide-free component of these intercumulus spaces is partially or completely infilled with crystallization products of highly fractionated residual trapped liquid derived from the interstitial liquid of the original crystal mush; these intergrowths typically develop as 'caps' above the globules. Similar partially-filled cavities are well known within basaltic and komatiitic lava flows and are referred to as 'segregation vesicles'; they have also been observed as caps above sulfide globules in quenched dolerite dyke margins in other localities. In the Norilsk-Talnakh intrusions, where the caps are incompletely filled by magmatic material the remaining space is occupied by amygdaloidal linings, which in some cases include anhydrite. These relationships provide evidence that the caps represent original gas bubbles and the close association with the sulphide globules arises from the strong tendency for sulphide droplets to attach to vapour bubbles in magmas. The original outlines of the vapour–bubble pairs are preserved by the rigidity of the surrounding crystal framework, which is interpreted to have developed largely by simultaneous *in situ* nucleation and growth of olivine and clinopyroxene on the basis of detailed textural observations. Pressure increase during solidification coupled with gas filter pressing forced residual silicate melt into the bubbles, while gas filter pressing and vapour–liquid capillary attraction drove differentiation of the droplets themselves. Whether the globules were deposited already attached to bubbles, or whether the bubbles were generated by volatile saturation within the crystal mush after deposition, cannot be determined definitively, but the geometry of flattened bubble–droplet pairs tends to favour the former option. The distinctive nature of the Norilsk globular ores, along with other unusual aspects of these deposits, is interpreted to be the result of low confining pressures and syn-crystallization degassing, an unusual condition in intrusion-hosted magmatic sulfide ores.

Key words: cumulates; droplets; magmatic ore deposits; nickel sulphides; vesicles

INTRODUCTION

The globular sulphide ores of the Norilsk-Talnakh Ni–Cu–PGE camp have long been recognised as accumulations of magmatic sulphide liquid droplets (Kotulskii, 1946; Godlevsky, 1959; Urvantsev, 1972; Dyuzhikov *et al.*, 1988) and are among the best-preserved examples of this type in nature. They form part of the enormous accumulation of strongly PGE-enriched Ni–Cu sulphide ores within the distinctive chonolith-style intrusions of the Norilsk-Talnakh ore camp, associated with the vast outpouring of basaltic magma known as the Siberian Large Igneous Province (Genkin *et al.*, 1982; Distler *et al.*, 1988; Dyuzhikov *et al.*, 1988; Naldrett, 1989, 2004; Fedorenko, 1994; Naldrett & Lightfoot, 1999; Li *et al.*, 2009; Lightfoot & Zotov, 2014; Malitch *et al.*, 2014; Ryabov *et al.*, 2014; Krivolutskaya *et al.*, 2018*b*).

The globular sulphides (Fig. 1) are most prominently developed within the 'picritic gabbrodolerite' layers of the host intrusions, interpreted in numerous previous studies as layers of olivine orthocumulate (Likhachev, 1994; Czamanske *et al.*, 1995; Krivolutskaya *et al.*, 2018*a*). The globules are characterised by very consistent and regular internal differentiation into Cu-rich (upper) and Cu-poor (lower) layers at a scale of a few mm (Natorkhin *et al.*, 1977; Czamanske *et al.*, 1992; Distler *et al.*, 1996; Barnes *et al.*, 2006), this being one of the best documented examples in nature of magmatic differentiation of sulphide liquids (Czamanske *et al.*, 1992; Barnes *et al.*, 2006). Another distinctive but less widely recognised feature is the association of the droplets with silicate 'caps'. These occupy original voids in the host cumulus crystal framework, now filled by silicate and other minerals and in many cases also containing amygdales. These features have been interpreted as segregation vesicles (Smith, 1967; Le Vaillant *et al.*, 2017), formed by migration of silicate melt into the space originally occupied by vapour bubbles attached to sulphide liquid droplets within a mushy cumulate pile. The close association between droplets and bubbles has been interpreted as the consequence of the strong tendency of coexisting vapour and sulphide liquid phases within silicate magmas to attach to one another owing to capillary (surface tension) effects (Mungall *et al.*, 2015). Le Vaillant *et al.* (2017) suggested that this association may have contributed to an important kill mechanism in the precisely simultaneous Permo-Triassic mass extinction (Burgess & Bowring, 2015), related to a sudden flux of vapour-transported nickel into the atmosphere, a consequent population bloom of methanogenic micro-organisms (Rothman *et al.*, 2014; Rampino *et al.*, 2017) and the environmental consequences thereof.

In this contribution, we document the textural associations between the sulphide globules and the infillings of the associated segregation vesicles in the broader context of the crystallization history of the host cumulate rocks. Using the technique of high-resolution X-ray fluorescence element mapping, we show that these infillings record the advanced *in situ* differentiation of residual trapped liquid within the so-called picritic gabbrodolerites and taxites of the Norilsk 1, Talnakh and Kharealakh intrusions, and evaluate alternative explanations for the mechanisms that generate the simultaneous advanced differentiation of both silicate and sulphide melt components. We further consider the implications for ore forming processes in one of the most valuable ore camps of any type on Earth and more broadly for the physical dynamics of sulphide liquid droplets.

GEOLOGICAL SETTING

The geological setting of the Norilsk-Talnakh orebodies within the Siberian LIP (Fig. 2) has been extensively documented. The brief summary presented here is based on a variety of sources (Dyuzhikov *et al.*, 1988; Naldrett *et al.*, 1992; Czamanske *et al.*, 1995; Naldrett & Lightfoot, 1999; Lightfoot & Zotov, 2014; Malitch *et al.*, 2014; Ryabov *et al.*, 2014; Sluzhenikin *et al.*, 2014; Krivolutskaya *et al.*, 2018a, 2018b). The ores are associated with a particular suite of elongate, roughly tube-shaped, broadly conformable intrusions termed chonoliths, possibly forming the thickened feeder pathways of regional-scale channelised sills, associated with a specific time period during the evolution of the LIP volcanism when strongly chalcophile-element-depleted lavas gave way to normal undepleted lavas (Naldrett *et al.*, 1992; Brugmann *et al.*, 1993). Large volumes of the Siberian LIP were emplaced as subvolcanic intrusions, but only a very small proportion have the distinctive tube-like chonolith facies and only these contain significant economic orebodies. The largest accumulations are associated with two of these intrusions, the Talnakh and Kharealakh intrusions, with a greatly subordinate but still large resource within the Norilsk 1 intrusion. All three of these bodies contain globular ores.

The Norilsk 1, Talnakh and Kharealakh intrusions are all located close to the presumed feeder structure called the Norilsk-Kharealakh Fault, coinciding spatially with the maximum thickness of the chalcophile-element-depleted Nadezhdinsky Basalt suite (Fedorenko, 1994; Krivolutskaya, 2014). Together, these intrusions comprise a small proportion (a few percent by volume) of the total volume of intrusions in the region and exemplify one of the fifteen types that have been identified. We refer to the three mineralised intrusions from here on as the 'ore-bearing intrusions'.

The ore-bearing intrusions occupy successively higher positions in sedimentary strata within 650 m of the contact between the Tungusskaya series of Middle Carboniferous–Upper Permian sediments, containing abundant coal beds and the flood basalt sequence. The Kharaelakh intrusion intrudes Lower to Middle Devonian, marine sedimentary rocks including

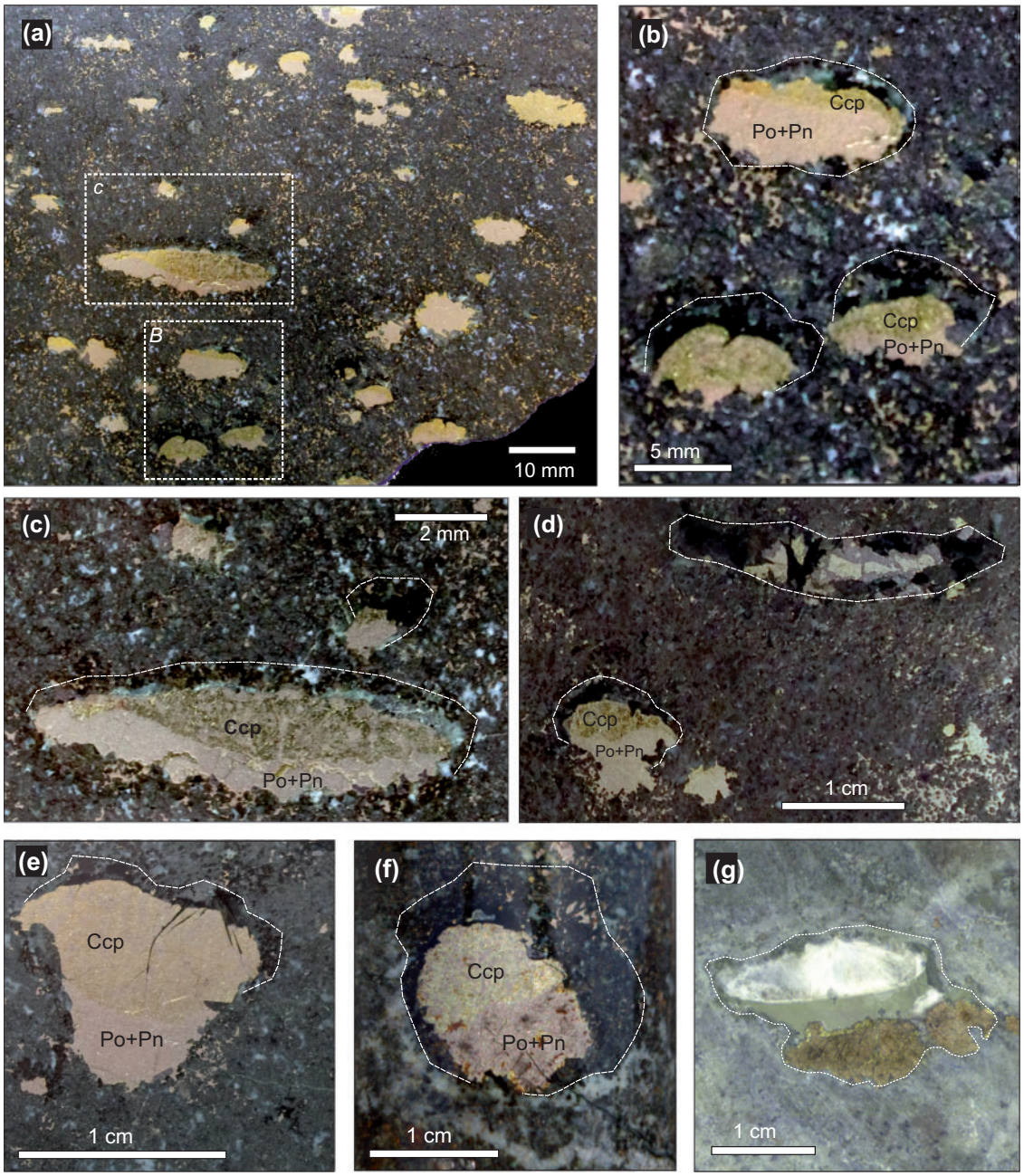

Fig. 1. Norilsk-Talnakh sulfide globules, polished slabs and drill cores. Photographs of museum samples. (a–c) Polished slab from Kharealakh intrusion. Strongly flattened large globules with outlines of silicate caps shown in white (b and c) in a matrix of picritic gabbrodolerite (olivine orthocumulate). Note that the larger globules are more flattened than the smaller ones. Disseminated interstitial sulfide is also present throughout. (d, e) Similar, Norilsk 1 intrusion. Globule in upper right of (d) is probably an intersection with the outer edge of a capped globule showing intergrowth with oxide phases; globule in lower left shows 'leakage' into disseminated interstitial sulfide beneath; typical feature of irregular interstitial lower contact compared with smooth meniscus-like upper contact. (f) Drill core, Kharealakh intrusion, capped globule associated with siliceous granophyre patch in taxitic gabbrodolerite. (g) Vesicular sample from upper taxitic layer of Norilsk 1 intrusion, showing a compound amygdale occupied by zeolite (white) above an amorphous Fe-silicate (grey-green) attached to a sulfide globule (below) within a fine-grained plagioclase-rich dolerite; sample from Marina Yudovskaya and Sergei Sluzhenikyn.

evaporites and the Talnakh intrusion intrudes Middle Carboniferous to Lower Permian sedimentary rocks (Figs 2 and 3). The Norilsk I intrusion straddles the Tungusskaya series/basalt contact, cutting the lower three of the eleven suites of the volcanic sequence at its north end and the lower six to the south. All were emplaced at shallow depths compared with most other known mafic intrusion-hosted magmatic sulphide deposits (Fig. 3), as a consequence of which they contain locally abundant amygdales (Spiridonov, 2010), particularly within the upper zone of the Norilsk 1 intrusion (Fig. 1g).

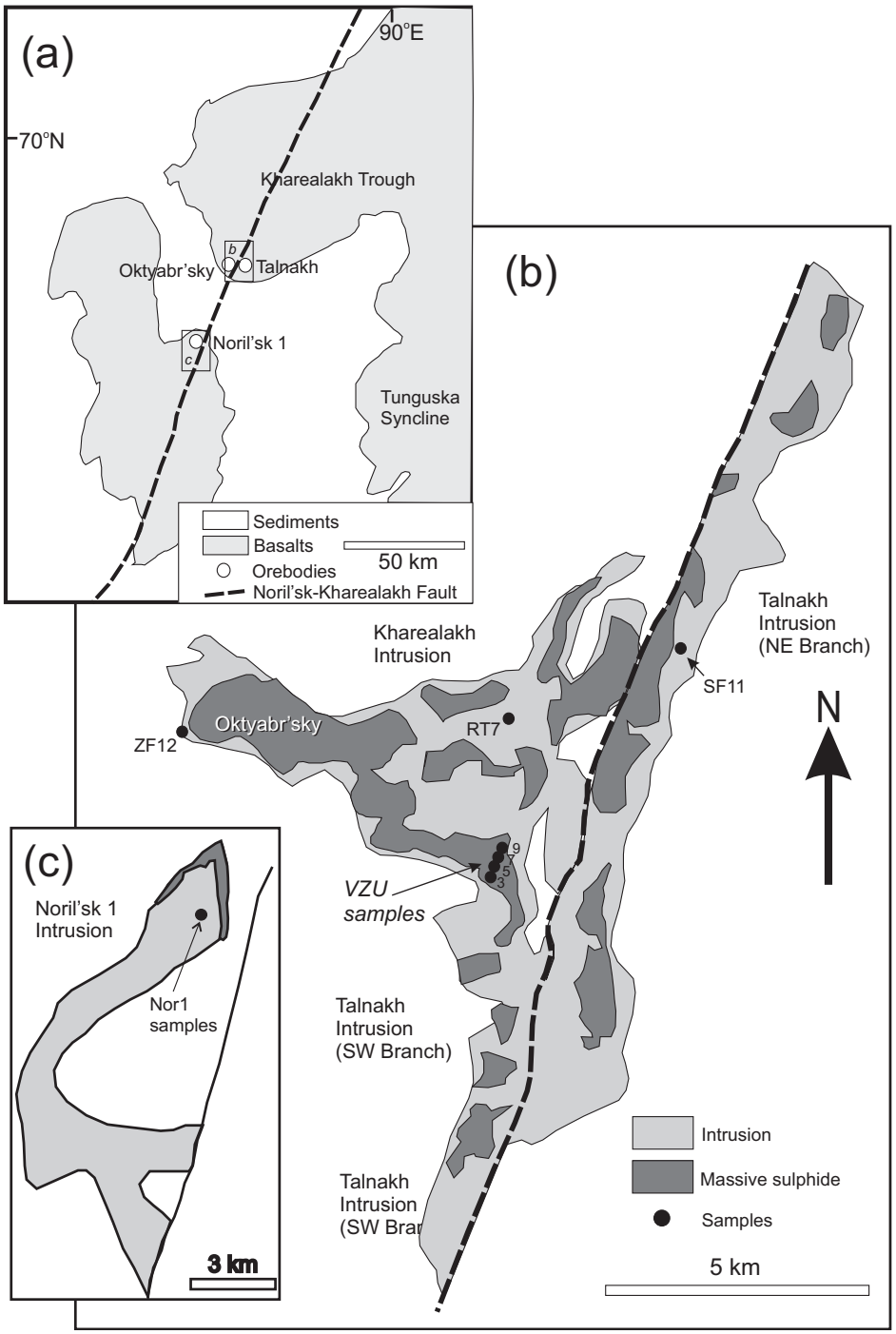

Fig. 2. (a) Location map, (b) detailed and (c) regional Noril'sk and Talnakh area maps modified from Naldrett (2004) and Sluzhenikin *et al.* (2014), with sample locations. Name 'Oktyabr'sky' refers to the ore deposit within the Kharealakh intrusion.

Summary description of the intrusions

All three of the ore-bearing intrusions are elongate sills, with a distinct lateral 'wing' in the case of Kharealakh, differentiated from picritic gabbrodolerite with an olivine orthocumulate texture to magnetite gabbro and leucogabbro, and all containing economic disseminated, massive and semi-massive ores (Naldrett, 2004; Lightfoot & Zotov, 2014; Sluzhenikin *et al.*, 2014). The main bodies of Talnakh and Kharealakh, but not Norilsk 1, are flanked by one or two much thinner, less differentiated and more laterally extensive dolerite sills. The Kharealakh intrusion tapers into a series of multiple thin sills at its western termination (Krivolutskaya *et al.*, 2018*b*). All three intrusions show laterally discordant relations with their country rocks, suggestive of a process of erosive emplacement; space was created by

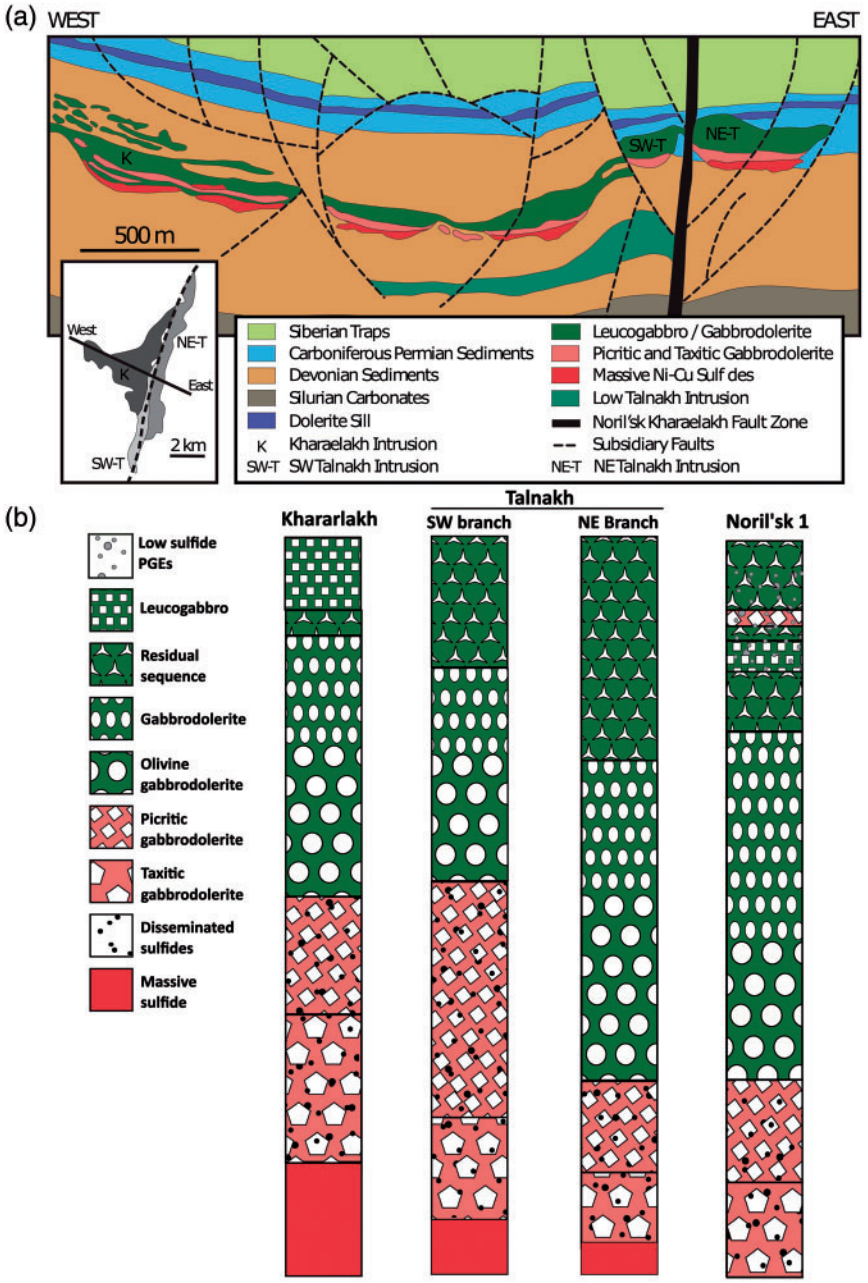

Fig. 3. (a) Simplified cross section through Talnakh and Kharealakh intrusions, after Lightfoot & Zotov (2014). (b) Summary of main stratigraphic subdivisions of the ore-bearing intrusions after Czamanske *et al.* (1995).

removal of sediment, rather than by lifting of the roof (Godlevsky, 1959; Urvantsev, 1972; Naldrett, 1999, 2004; Ryabov *et al.*, 2014).

The Norilsk-area intrusions have attracted a unique terminology, including the rock names 'taxite' and 'gabbrodolerite' that are not widely used anywhere else. These terms are used here to maintain consistency with the existing large body of Norilsk literature. Gabbrodolerites are essentially poikilitic to ophitic gabbros (plagioclase, clinopyroxene, no orthopyroxene), too coarse grained to be called dolerites; picritic gabbrodolerites are the same rock with cumulus olivine in excess of 25 modal %. The term 'olivine gabbrodolerite' is also in use, meaning an olivine gabbro where olivine forms oikocrysts to interstitial phases only (Czamanske *et al.*, 1995).

The three intrusions show strong and broadly similar internal differentiation (Czamanske *et al.*, 1995; Krivolutskaya *et al.*, 2001, 2018a; Sluzhenikin *et al.*, 2014), having a basal chilled dolerite zone, overlain in turn by taxitic gabbrodolerite, picritic gabbrodolerite with decreasing olivine content upward, transitional

into olivine gabbrodolerite, quartz- and magnetite-bearing gabbrodolerite, leucocratic gabbro and upper contact gabbrodolerite (Fig. 3).

Globular ores occur in three main settings within the intrusions. Most are found within picritic gabbrodolerite layers in the lower parts of the intrusions. These layers are characterised by high MgO contents, up to about 25% (Arndt *et al.*, 2003; Krivolutskaya *et al.*, 2018*b*), well in excess of the likely parent liquid MgO content, have distinctive poikilitic textures and are, therefore, recognisable as olivine orthocumulates, described in detail below. The samples described in this contribution are predominantly from these picritic gabbrodolerites. Less regular and typically larger sulphide blebs occur within the olivine-bearing taxitic gabbrodolerite layers that underlie the picritic gabbrodolerites. Their variable grain size is accompanied by the presence of irregular patches of felsic material and also fine-grained olivine- and pyroxene-bearing aggregates, interpreted as incompletely digested country rock inclusions (or the restites derived by partial melting thereof). The third setting is within similar olivine-bearing taxites, with high proportions of assimilated country rock and chromite-rich patches or schlieren, found near the tops of the intrusions. The sulphide blebs in this setting tend to be smaller and have a strong association with amygdales (Distler *et al.*, 1999). These rocks are very strongly enriched in PGE (Distler *et al.*, 1999; Sluzhenikin *et al.*, 2014) at low sulphide contents.

METHODS AND MATERIALS

XFM imaging

Microbeam X-Ray Fluorescence mapping (XFM mapping) was carried out using two different techniques: at coarse (~40 micron) spatial resolution using a desktop Bruker Tornado instrument and at fine (~2–4 micron resolution) using the Maia detector array on the XFM beamline at the Australian Synchrotron (AS) (Paterson *et al.*, 2011). The Bruker Tornado^{TM} desktop instrument is equipped with a rhodium target X-ray tube operating at 50 kV and 500 nA without filters and an XFlashVR silicon drift X-ray detector. Images are processed using the Bruker ESPRIT software, which gives standardless semi-quantitative analyses for elements heavier than Na, with estimated detection limits of around 1000–2000 ppm for first-row transition metals under the given operating conditions and dwell times. Concentration data were calibrated for selected samples by comparison with wavelength-dispersive spectrometry (WDS) electron microprobe analyses, as described by Barnes *et al.* (2016*c*). Maps were created using a (nominally) 25 μm spot size on a 40 μm raster with dwell times of 10–20ms per pixel. Maps are represented as unquantified background-corrected peak height data for Kα peaks for each element, normalised to the maximum peak height for that element in each sample. These maps were converted to phase maps by a process of selective masking using the colour selection tool in Adobe Photoshop^{TM}.

Maia-XFM data were collected at the AS using the Kirkpatrick Baez mirror microprobe end-station. This provides a monochromatic 2 μm beam spot size for energies in the range 4–20 keV. Equipped with the Maia 384 detector array, the XFM beamline can acquire data at 2 μm resolution from 384 detectors simultaneously over areas of several square centimetres with count rates of 4–10 M s^{-1}, and energy resolution of 300–400 eV. These spectra are then processed by the GeoPIXE software into element concentrations represented as maps of quantified element concentrations based on standardless correction of raw count data (Kirkham *et al.*, 2010, Ryan *et al.*, 2014).

High-resolution X-ray tomography (HRXCT)

Selected samples (~ 2·5 cm in diameter and ~6 cm in length) were scanned using a Zeiss® XRM500 3 D X-ray microscope installed at the Australian Resources Research Centre, CSIRO Mineral Resources, Perth, Australia. The instrument was set-up (source and detector positions, source filtering, voltage, energy) for each sample to maximize the contrast between the different mineral phases present in the samples. The voxel size was kept constant to 13·2 μm between the different samples to allow comparison of quantitative measurements between the different samples. For each sample, four scans were acquired to cover the entire length of each sample. A total of 1601 projections were recorded for each scan (i.e. 0·22 ° rotation of the sample between each projection). Artefacts such as ring artefacts or beam hardening were reduced during acquisition (dynamic removal of ring artefacts) or corrected for during the reconstruction procedure. Each reconstructed scan was stitched using 3 D algorithms to create a single grid covering the entire sample. Each reconstructed dataset was processed using Avizo 9·5 ® (ThermoFisher) and Matlab® (MathWorks) softwares. The sulphides were segmented using the procedure described in Godel (2013), whereas quantitative measurements (size, morphology, orientation and topology) and associated statistics were computed using methods similar to those used by Godel *et al.* (Godel *et al.*, 2013a, 2017).

Low resolution medical CT images were collected using a SOMATON Definition AS Medical CT Scanner at ARRC and processed using Avizo 9·5 ®, following the protocols described by Barnes *et al.* (2016*a*).

Samples studied

A total of 16 samples (Table 1) were investigated and imaged from the ore-bearing intrusions (Table 1). Of these, detailed X-ray maps and in some case 3 D X-ray datasets are presented in detail for representative rock types from each intrusion.

Table 1: List of imaged samples

Sample	Intrusion	Rock-type	Description	Sulphide globules %	Sulphide diss-int %[1]	Ratio int/total[2]	Est. ratio cap/globule (area)[3]
KH2	Kharealakh	PGD	Typcal PGD with abundant flattened globules, mostly with large (1:1) caps	26·7%	8·4%	23·9%	100·0%
RT7-147	Kharaelakh	PGD taxitic	Typical PGD with fine xenoliths, large partially coalesced globules plus fine interstitial sulf.	9·7%	4·5%	31·7%	n.d.
VZU-3B	Kharaelakh	PGD	Typcal PGD with abundant flattened irregular globules, mostly with caps, extensive growth of cpx into caps	13·9%	2·1%	13·0%	75·0%
VZU-5B	Kharaelakh	PGD	Typcal PGD with abundant flattened irregular globules, mostly with caps, extensivee growth of cpx into caps	1·5%	2·2%	59·6%	
VZU-5A	Kharaelakh	PGD	Typcal PGD with abundant flattened irregular globules, mostly with caps, extensice growth of cpx into caps	9·4%	3·0%	24·0%	80·0%
VZU-7	Kharaelakh	PGD	PGD with skeletal olivine, irregular caps hard to discern in 2D images	6·2%	3·2%	34·5%	n.d.
ZF12-391.7	Kharaelakh	PGD	PGD with large branching harrisitic olivine grains	n.d.	n.d.		
ZF12-394.0	Kharaelakh	PGD	PGD with fine grained xenoliths, patches of associated coarse skeletal olivine	n.d.	n.d.		
Nor1-1	Norilsk 1	PGD	PGD, large spherical globules,	15·5%	6·4%	29·3%	
Nor1-2	Norilsk 1	Taxitic GD	Plag framework, vari-textured, fine xenoliths, coarse strongly Cr-zoned cpx, no olivine, sulphide coarse interstitial	n.d.	n.d.		
Nor1-3	Norilsk 1	PGD	Single large globule (incomplete) with large ~1 cm near-spherical silicate cap	8·3%	2·3%	21·8%	80·0%
Nor1-4	Norilsk 1	PGD	Single large globule (incomplete) with large ~1 cm near-spherical silicate cap	4·1%	0·7%	14·4%	60·0%
Nor1-5	Norilsk 1	PGD	Vari-textured, coarse plag, minor olivine in strongly zoned cpx,	13·3%	2·3%	15·0%	
Nor1-6	Norilsk 1	PGD	Vari-textured, coarse plag, minor olivine in strongly zoned cpx,	n.d.	n.d.		
CML-Nor1	Norilsk 1	PGD	Typical PGD with abundant flattened globules, several with large caps	25·7%	6·1%	19·1%	60·0%
Czam-Slab	Norilsk 1	PGD Vari-textured (taxitic)	PGD with fine grained xenoliths, patches of associated coarse skeletal olivine	5·8%	1·8%	23·5%	n.d.

[1]modal proportion of disseminated sulphide in sample; [2]ratio of area of interstitial to globular sulphide; [3]estimated proportion of area of silicate cap to globule. All values determined from 2D images. PGD, picritic gabbrodolerite.

RESULTS

Mode of occurrence of sulphide globules

Globular ores are coarse disseminated ores containing up to around 10% sulphide at decimetre scale, in which sulphides form aggregates on a scale of mm to cm, similar to, or larger than, the characteristic grain size of the enclosing silicates (Barnes *et al.*, 2017*b*). Such ores have commonly been referred to as 'blebby', but Barnes *et al.* (2017*b*) recommend that 'blebby' should refer to sulphide aggregates of any geometry, whereas 'globular' should be used as a specific term for convex sub-spherical blebs, as distinct from 'interstitial blebs' where sulphides primarily occupy the interstitial space between touching networks of silicate crystals. Both types, globular and interstitial blebs, are present in the same Norilsk-Talnakh samples (Fig. 1) and have been imaged in selected samples by high-resolution X-ray computed tomography (HRXCT, Fig. 4). Blebs in picrodolerites tend to be subspherical, while those in the underlying taxitic gabbrodolerites tend to be larger and more irregular.

Characteristically the sulphides occur within a framework of silicate crystals, most commonly olivine, but also plagioclase in varying proportions. Commonly, the sulphide globule partially occupies sub-spherical intercumulus spaces within the 3 D framework defined by the touching cumulus grains, usually olivine; the sulphide globule occupies the base of the space, the upper sulfide-free part of which (described in detail below) is referred to as the 'silicate cap'. In some cases, as noted by Le Vaillant *et al.* (2017) (e.g. Fig. 1g), this cap is in part, or in whole, an amygdale, occupied by low temperature minerals including carbonates, clays, anhydrite and chalcedonic silica, but more commonly it is completely occupied by late crystallising magmatic silicate and oxide minerals and is interpreted by Le Vaillant *et al.* (2017) as a filled segregation vesicle, exactly analogous to those commonly reported in basalts (Smith, 1967; Anderson *et al.*, 1984). Size distributions of globules were reported by Robertson *et al.* (2015) from low resolution medical CT scans on a subset of three of the samples studied here; they conform to log-linear particle size distributions with intercepts at zero particle size of 1–10 particles per mm^3 and predominant particle sizes in the range from 1 to 15 mm (expressed as equivalent sphere diameters). In the samples imaged by HRXCT (Figs 4 and 5), the globules are enclosed within larger touching frameworks of finely interconnected interstitial sulphides, extending around the globules in all directions, discussed in detail below. The globular and interstitial sulphide components appear to be isotopically and compositionally identical (Le Vaillant *et al.*, unpublished data).

Considerable diversity exists within the Norilsk globules, even within the same hand sample (Fig. 1), but some typical characteristics can be identified. The simplest type is a variably flattened lens or oblate spheroid (Fig. 1a and c) beneath a smaller silicate cap that follows the upper contour of the globule. In the samples with the most extensive flattening (Fig. 1) larger globules tend to be more flattened than smaller ones, although this relationship appears to be restricted to globules larger than about 1 cm in maximum diameter. There is no evidence of deformation of the silicate crystal framework around flattened globules. Outlines are typically circular in the plane of layering, at right angles to the flattening direction (Figs 4 and 5). Some more irregular globules, particularly in the taxites rather than in the more equigranular picrodolerites, range from rounded concave lower contacts (Fig. 1e, left) to irregular lower boundaries marked by penetration of sulphide into the intercumulus framework over a few grain diameters in 2 D (Fig. 1d and e right); the 3 D images (Figs 4 and 5) reveal that these downward penetrating sulphides form part of the extensive 3 D interstitial networks. The upper contacts of the globules are invariably concave-up, defined by the contact between chalcopyrite and the silicate cap mineralogy, and either in form of a smooth meniscus (Fig. 1b and d–f) or as a surface modified by the development of faceted crystals of chalcopyrite (Fig. 1e, right). The contact between the chalcopyrite-rich upper part of the globule and the pyrrhotite–pentlandite rich lower part is in most cases a smooth concave-down meniscus (e.g. Fig 1c and e) or in some cases a smooth horizontal plane (Fig. 1b).

In the following sections, we describe representative samples from two of the three mineralised intrusions. We document the petrology of the host silicate (or silicate-oxide) cumulate framework, the interstitial phases, the silicate cap filling, the textural relationships of the sulphide globules to the non-sulphide minerals and the internal differentiation of the globules themselves.

Norilsk 1 intrusion globular ores

Vari-textured (taxitic) picritic gabbrodolerite

The spectacular polished slab imaged in Fig. 6 is a globule-rich sample best characterised as a xenolith-bearing vari-textured picritic gabbrodolerite, illustrating many of the common features found in such rocks in all three intrusions. This rock type is typical of the transition between the picritic gabbrodolerite and the underlying taxitic gabbrodolerite. The imaged surface is cut approximately parallel to primary layering, such that silicate caps and internal differentiation of the globules are not well displayed, but the heterogeneity of the silicate matrix is evident. Numerous irregular, fuzzy-edged patches of feldspathic material (marked by the presence of K-feldspar, Fig. 6b) represent partially digested sedimentary xenoliths. A second population of calc-silicate xenoliths composed of fine grained olivine and Ca-silicate minerals is also present (Fig. 6c and d) and is closely associated with the presence of large skeletal olivine grains (Fig. 6d). Interstitial clinopyroxene is present as small oikocrysts throughout the sample (except in the xenoliths) and shows two distinctive

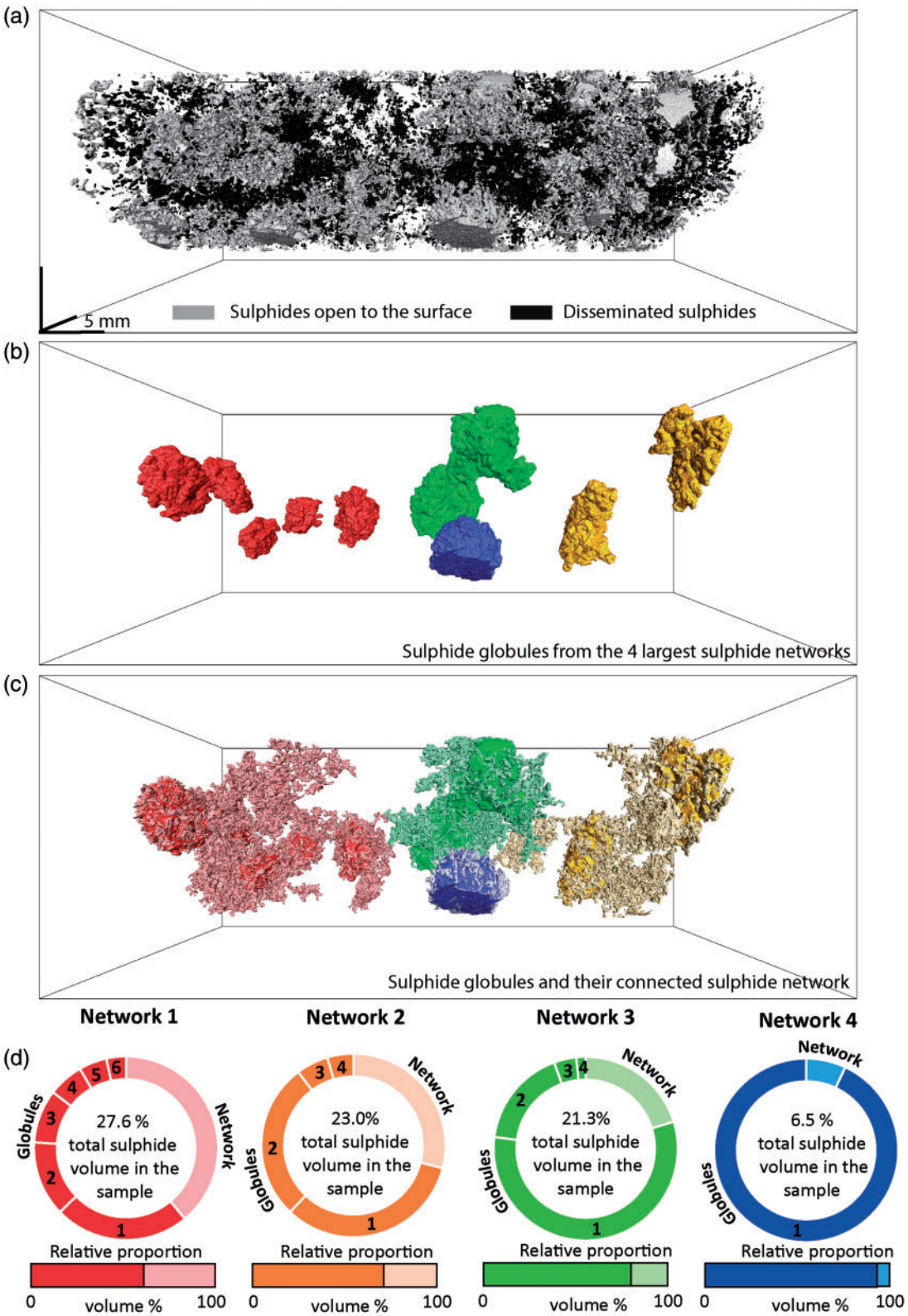

Fig. 4. High resolution XRCT images of sample VZU3. (a) Grey scale volume render of the entire sample showing sulphide networks connected to the sample surface (lighter grey) and finer sulphides entirely encompassed within the sample. (b) Sulphide globules according to connectivity (i.e. all globules lying within the same interconnected 3D network have the same colour). (c) The four largest sulphide networks showing globules (solid) and interstitial networks (transparent). (d) Relative volume proportions of the globules and interstitial sulphide for each of the four largest networks.

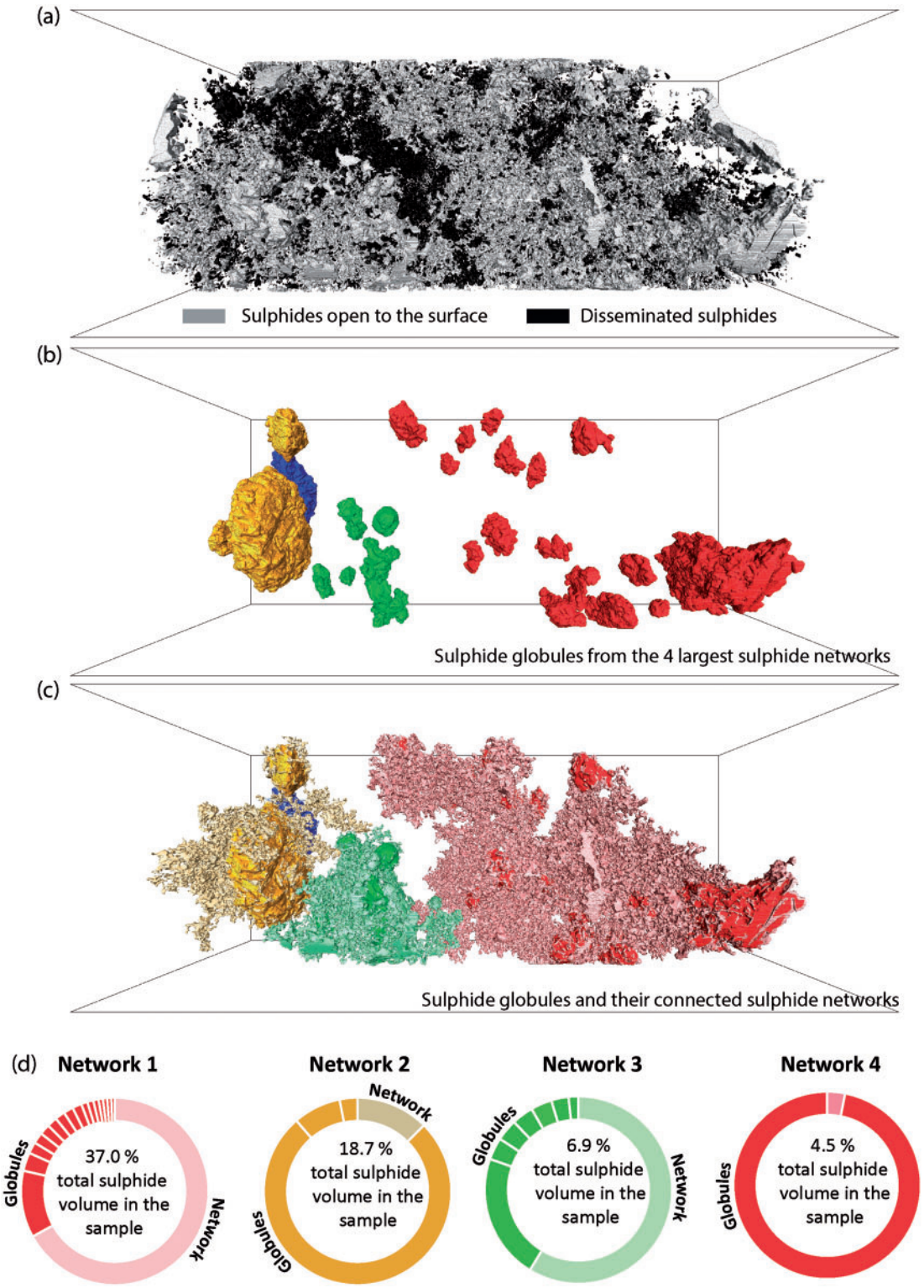

Fig. 5. High resolution XRCT images of sample RT7-147, as in Fig. 4.

characteristics found in every picritic rock type examined so far for all three intrusions: distinct Cr-enrichment in the cores of the grains and presence of very small olivine chadacrysts within the Cr-rich cores.

Picritic gabbrodolerite

Images from two samples of picritic gabbrodolerite (Fig. 7) show a number of characteristic features. The globules vary from oblate to spherical, in some cases

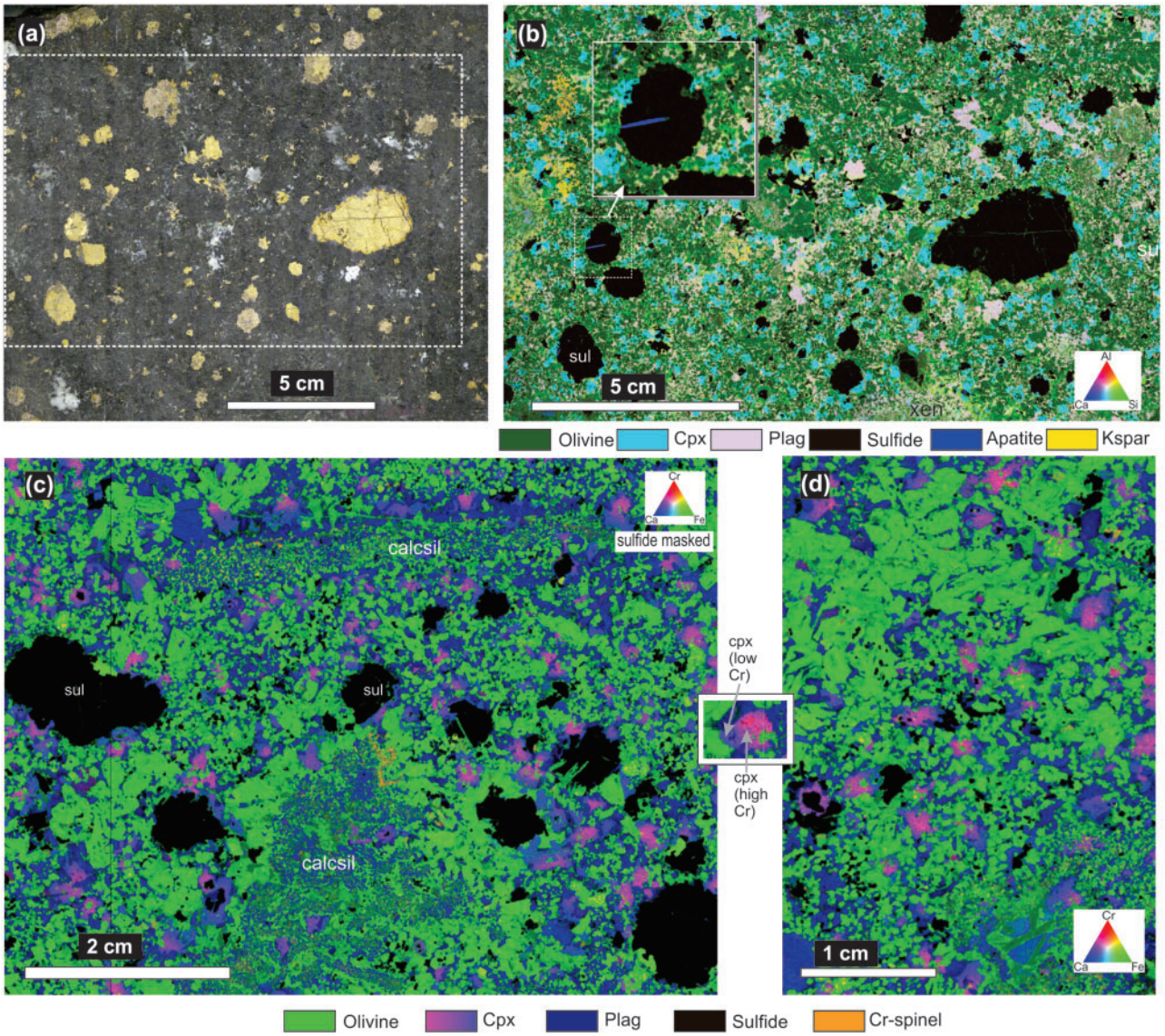

Fig. 6. Sample Czam-slab. Taxitic picritic gabbrodolerite (Bear Pit, Norilsk 1 intrusion). (a) Polished slab and (b–d) Tornado microbeam XRF element maps; (b) same area as (d). Al (red), Si (green), Ca (blue), showing fine-grained feldspathic patches (pale pink) interpreted as partially digested xenoliths (xen); inset enlargement shows needle of apatite (blue) enclosed within sulphide globule. (c, d) XRF maps of reverse side of same slab, Cr (red), Fe (green), Ca (blue), with sulphides masked in black. (c) Calc-silicate xenoliths (calcsil) consisting of fine grained olivine and Ca-silicates, rimmed by equant and skeletal olivine and zoned cpx. (d) Same sample, detail of coarse skeletal olivine and zoned cpx. Note common presence of very small olivine inclusions in the Cr-rich cores of some cpx grains. Cr scale in cpx ranges from about 1% (pink) to 0·4% (blue).

(Fig. 7a and b) showing evidence of partial coalescence. Not all show silicate caps. The globules are embedded within a continuous framework of cumulus olivine grains with interstitial to poikilitic clinopyroxene, commonly with Cr-enriched cores, interstitial plagioclase and some finer grained domains that may represent remnants of xenoliths. The silicate caps are most easily recognisable as sub-spherical voids within the olivine framework (Fig. 7d and e). Ti-rich phlogopite, Fe–Ti oxide phases and Ti-enriched amphibole are developed around the margins of the silicate caps, which are otherwise filled with mixtures of fine grained amphibole, chlorite, unidentified probable clay phases and rarely calcite and/or anhydrite. Chalcopyrite in the upper segments of the sulphide globules is commonly finely intergrown with pyrrhotite and pentlandite in a lamellar to symplectic intergrowth. In this and most other Norilsk 1 samples, the top contact of the sulphide globule is lined with Ti-rich oxides and in some cases with Ti-rich phlogopite (Fig. 7e and f) which commonly penetrates into the sulphides.

Three dimensional images of droplets from Norilsk 1 (Figs 8 and 9d) show a range in shape within samples from sub-spherical to irregular, reflecting varying

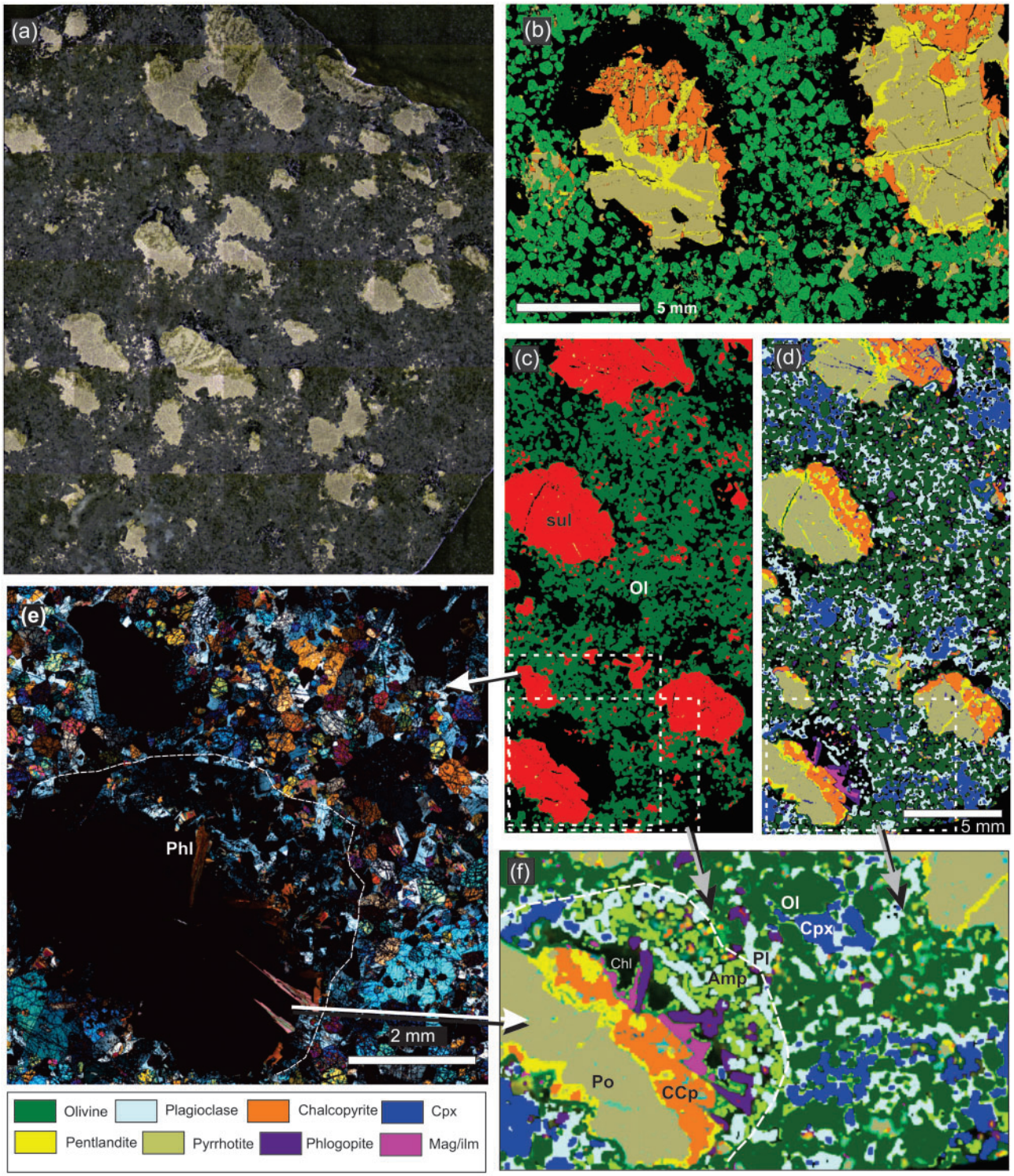

Fig. 7. Globular ores in picritic gabbrodolerites, samples CML-Nor1 (a–d) and Nor1-1 (e, f), Bear Creek Pit, Norilsk 1 intrusion. (a) Polished slab; (b–d) and (f) are Tornado XRF maps and derived phase maps showing consistent arrangement of sulfide phases within droplets. (b, c, d) Phase maps showing relationship of sulphide globules (red in (c)) to olivine cumulus framework. (e) Photomicrograph of capped globule in lower left of (c) and (d); note lining of contact between droplet and silicate cap with phlogopite and Fe–Ti oxides, interior of cap is fine-grained amphibole, silica and/or clay. (f) Detailed Tornado phase map of the same area.

degrees of connection between globules and interstitial sulphides, as well as limited coalescence. Interstitial disseminated sulphides (Fig. 8) account for a small proportion of the total area of sulphide: average 22% ± 6% (one standard deviation on eight samples, measured by image analysis on Tornado images).

The silicate cap imaged in Fig. 9c shows a hemispherical outline attached to a flat-topped differentiated

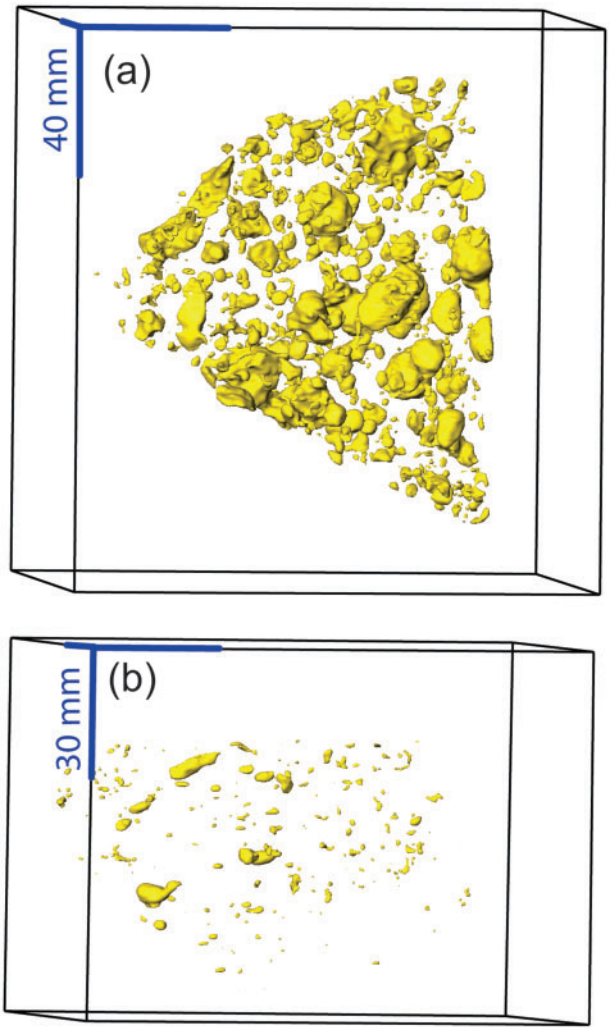

Fig. 8. Perspective views of 3D medical CT scan images of samples (a) Nor1-1 and (b) Nor1-2, Norilsk 1 intrusion. See Supplementary Data files for animations of the Nor1-1 image. Note that these images are at ~100 micron resolution and do not resolve the fine interstitial disseminated sulfide component.

globule (the bottom of the globule is missing from this sample), with the cap being outlined by the presence of a fine-grained Ti-rich Cr spinel rind. The top half of the cap is partially occupied by strongly zoned clinopyroxene grains, with Cr-rich cores and Ti-rich rims, developing as overgrowths on oikocrysts from within the olivine framework. This is a common feature in most of the samples studied from all three intrusions. The remaining space within this globule is filled with a highly porous, very fine grained unidentified phase mixture composed mainly of FeO and SiO_2 showing pseudomorphed quench (or possibly devitrification) textures; the volume around the residual anhydrite-filled amygdale (Fig. 9b) is probably altered glass. Both samples illustrated in Fig. 9 have a cumulus silicate framework defined by phases additional to olivine: plagioclase in Nor1-4, and olivine, chromite and plagioclase in Nor1-3 (see images previously published by Le Vaillant *et al.*, 2017). The top of the sulphide globule in Nor1-4 (Fig. 9a and b) shows a well-developed lamellar intergrowth of pyrrhotite and chalcopyrite, interpreted as the result of subsolidus unmixing of an intermediate solid solution (ISS), the crystallization product of the residual Cu-rich liquid from sulphide liquid fractionation.

Kharealakh intrusion

Globular ores in picritic gabbrodolerites from the Kharaelakh intrusion show many of the same features as those described from Norilsk 1, but some distinctive features were noted in particular samples and have been imaged using synchrotron XFM mapping as well as Tornado mapping and high-resolution XCT. These features are well preserved in samples VZU3 and RT7-147, which contain irregular flattened globules beneath oblate caps (Figs 4 and 5). These globules are embedded in an extensive network of interstitial disseminated sulphides accounting for 34–42% of the total sulphide volume; these are prominent in the 3D microCT images (Figs 4 and 5) owing to the high degree of interconnectivity at a scale of several cm (probably more, given that most of the networks imaged extend outside the surface of the samples). The sample also contains a large number but small aggregate volume (<1%) of small non-interconnected interstitial blebs ('stranded drops' in the terminology of Barnes *et al.*, 2017*a*). The irregular shape of the globules is largely controlled by moulding around plagioclase gains and around facetted, zoned clinopyroxene and Fe–Ti oxides (Fig. 12). Similar moulding around oxide and apatite grains is seen in sample KH2 (Fig. 10d–g).

The proportion of interstitial network sulphide to the total volume of sulphide in the combined network and globule, calculated from the high-resolution 3D images, varies from 3–66% (average 29·5% ± 23; Figs 4 and 5); this compares with mean values from 2D images of 22% and a standard deviation of 6% over 15 samples. Shapes and orientations of the sulphide blebs in the two samples for which high-resolution 3D images were collected are shown in Fig. 11. The globules range from spherical to disk shaped on the aspect ratio plots, but contrary to appearance in 2D, in some samples there is no significant correlation between shape and overall globule size in 3D; small globules are as likely to be spherical as larger ones (Fig. 11c and g) within the size range sampled in the 3D images. The orientation of the globules is plotted as a histogram of poles to the plane of maximum flattening, relative to an arbitrary reference direction, and shows strong shape-preferred orientation in both samples, with deviation of around 20–30 degrees covering 80% of the measurements. This is taken to reflect flattening into the original horizontal plane of deposition, with the deviation probably reflecting the roughness of the deposition surface at the scale of the globule size.

The matrix of the Kharealakh picritic gabbrodolerites is similar to that of the Norilsk 1 samples. Poikilitic

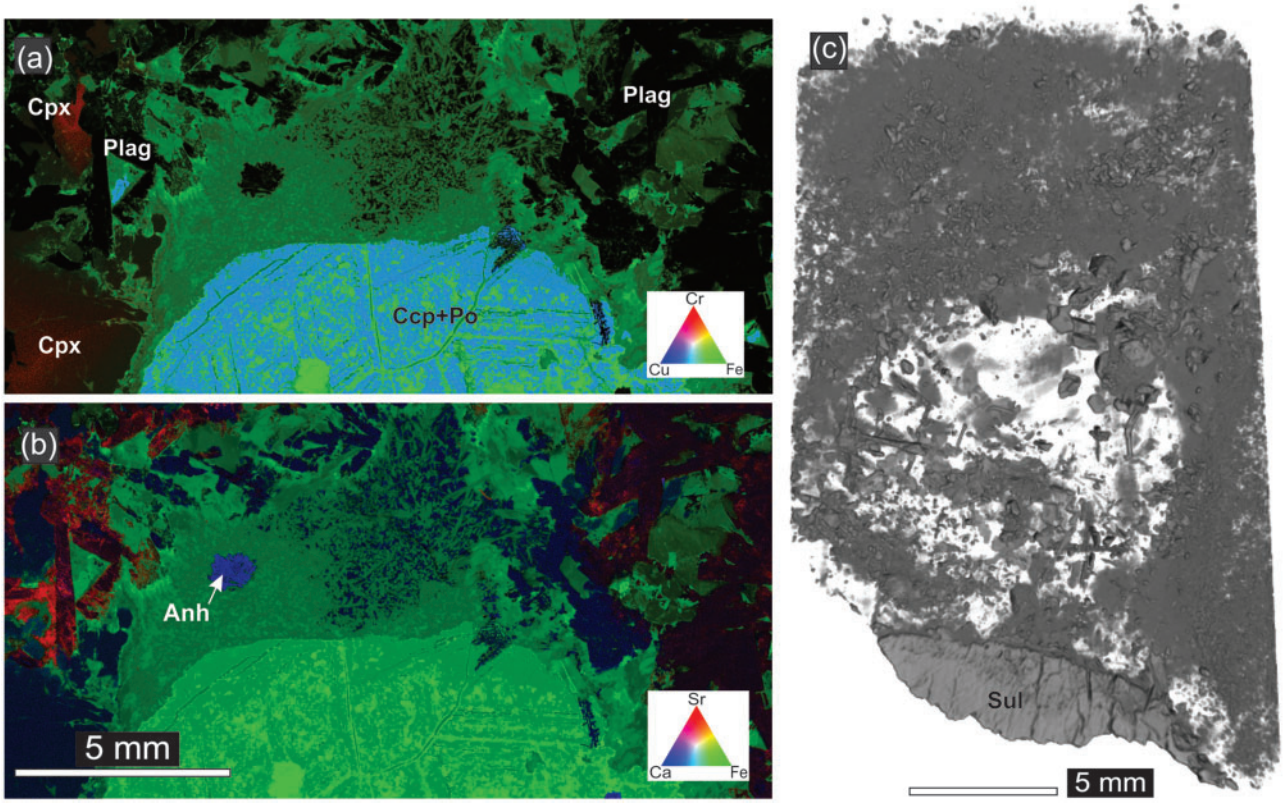

Fig. 9. (a, b) Maia XFM maps of a polished section and volume render (greyscale proportional to X-ray absorbance) of (c) 3D microCT scan of a thin-section billet of Norilsk 1 olivine-poor gabbrodolerite samples Nor1-4A (a, b) and Nor1-3 (c).

olivine orthocumulate textures are characterised by distinctly zoned clinopyroxene oikocrysts, with Cr-rich, Ti-poor cores and Ti-rich, Cr-poor rims, scattered disseminated Cr spinel, more abundant around the margins of the sulphides and silicate caps, and interstitial plagioclase and sulphide. Olivines within the Cr-rich cores of the pyroxene oikocrysts are distinctly finer grained than those outside (Fig. 12a–c). Subtle sector zoning defined by small variations in Cr content are evident in some oikocrysts, e.g. Fig. 12c. The strongest zoning is seen in the outer zones of clinopyroxene grains that extend into the cavities in the olivine framework. These zoned pyroxene rims form overgrowths on oikocrysts developed within the framework, and are now either surrounded by sulphide (Fig. 12d–f) or are embedded within the hydrous silicate components of the silicate caps, as in the Norilsk 1 sample illustrated in Fig. 9a and b. Pyroxenes are typical augites in composition (Table 2), zoned from $\sim$ 0·9% Cr_2O_3, 2·8% Al_2O_3 and 0·5% TiO_2 in the cores to 0·4% Cr_2O_3, 0·9% TiO_2 and 2·2% Al_2O_3 in the outer rims (Table 2). In some cases (Fig. 12d and e) this zoning is oscillatory (Schoneveld *et al.*, unpublished data). The edges of the inter-olivine voids are commonly decorated by inward-growing Ti-rich phases including complexly zoned Ti-magnetite with Cr-rich cores (Fig. 12b and f), ilmenite, rutile and titanite. These phases are commonly almost completely enclosed in sulphides, which are moulded around all the other silicate and oxide phases including plagioclase.

A number of the Kharealakh intrusion samples (including VZU7 and ZF12-381.7) contain coarse-grained branching skeletal olivine grains (Fig. 13), similar to but somewhat more elongate than those noted above in the Norilsk 1 taxite sample (Fig. 6). These olivines have interstices occupied mainly by clinopyroxene and plagioclase. A detailed Maia-XFM map (Fig. 13e) shows that the interstitial clinopyroxene grains have the typical Cr-enriched cores. Fine grained chromite is a common accessory in these rocks, as inclusions in olivine and clusters of fine grains.

DISCUSSION

Crystallization of the picritic gabbrodolerites

Microtextures and grain size relationships between olivine and clinopyroxene oikocrysts (e.g. Fig. 12) provide some important insights into the crystallization mechanism of the olivine cumulates of all three ore-bearing intrusions. In all samples where poikilitic textures are observed, the olivine grains are distinctly finer grained inside the oikocrysts than outside. There is no reason to believe that there is a peritectic relationship between olivine and augite in these magmas and none of the standard low-pressure phase diagrams for mafic magmas predicts such a relationship, so this relationship is not attributable to reactive dissolution of olivine.

There are two opposing interpretations for the origin of poikilitic textures in cumulates. The first, following

Table 2: Average compositions of pyroxenes and olivines from VZU samples, Kharealakh intrusion

Sample	VZU3	VZU3	VZU3	VZU3	VZU3
n	4	2	10	18	111
Phase	Olivine	Opx	Cpx	Cpx	Cpx
Core/rim	core	core	core	rim	all
SiO_2	38·82	54·56	51·68	51·40	51·20
TiO_2	0·03	0·66	0·58	1·31	0·90
V_2O_5	0·00	0·00	0·00	0·00	0·00
Al_2O_3	0·01	0·95	2·66	2·03	2·29
Cr_2O_3	0·01	0·09	0·88	0·33	0·50
FeO	21·43	13·78	6·40	7·49	7·18
Fe_2O_3	0·00	0·00	0·00	0·00	0·00
MnO	0·31	0·34	0·17	0·23	0·21
MgO	39·80	27·48	16·08	16·33	16·24
CaO	0·19	1·85	20·48	19·54	19·75
Na_2O	0·01	0·05	0·29	0·34	0·32
K_2O	0·00	0·01	0·00	0·00	0·00
NiO	0·21	0·06	0·05	0·04	0·10
Total	100·82	99·81	99·27	99·04	98·69
Si	3·99	7·85	7·67	7·67	7·66
Al	0·00	0·16	0·46	0·36	0·41
Ti	0·00	0·07	0·06	0·15	0·10
Cr	0·00	0·01	0·10	0·04	0·06
Mg	6·10	5·90	3·56	3·63	3·62
Fe2+	1·84	1·66	0·79	0·93	0·90
Mn	0·03	0·04	0·02	0·03	0·03
Ca	0·02	0·29	3·26	3·12	3·17
Na	0	0	0	0	0
Catsum	11·98	15·97	15·93	15·93	15·94
Mg#(En/Fo)	76·80	78·04	81·74	79·54	80·10
Woll		3·64	42·80	40·62	41·18

conventional cumulus theory, is that oikocrysts grow in the pore space of a crystal mush pile at a temperature intermediate between the liquidus and solidus (Wager *et al.*, 1960; Wager & Brown, 1968). An alternative hypothesis (Fig. 14), following from the *in situ* growth ideas of Campbell (1978) and McBirney & Noyes (1979), is that oikocrysts are cumulus crystals crystallizing with olivine in a boundary layer at the contact between the magma and an advancing crystallization front. The poikilitic textural relationship in this view is akin to ophitic textures in dolerites; the poikilitic mineral grows fast from dispersed nuclei, relative to the enclosed chadacryst mineral that is growing slowly from many nuclei (Fig. 14). In this model, poikilitic textures are the result of competitive simultaneous growth of multiple cumulus phases and the textures inside the oikocrysts reflect the earliest stages of development of the cumulus framework (Mathison, 1987; Higgins, 1998).

A number of lines of evidence have been invoked by various authors in favour of the *in situ*, competitive growth hypothesis. Zonation in crystal size and habit from small, semi-skeletal chadacryst grains in the core of the host oikocryst, to larger, more subhedral morphologies towards the rim, has been documented in many intrusions (McBirney & Noyes, 1979; Mathison, 1987; McBirney & Hunter, 1995; Tegner & Wilson, 1995). Campbell (1968) demonstrated that oikocrysts of a particular mineral are commonly restricted to a limited stratigraphic interval just below the first appearance of that mineral as a conventional cumulus phase, suggesting that they formed *in situ* as cumulus phases from supersaturated liquids. The occurrence of dendritic chromite oikocrysts in komatiitic olivine adcumulates can only be explained in terms of simultaneous growth, with the poikilitic phase growing fast owing to supersaturation (Barnes & Hill, 1995; Barnes, 1998; Godel *et al.*, 2013*b*). Donaldson *et al.* (1973) described spectacular radiating branched plagioclase oikocrysts up to one metre in size in peridotites from Rum and concluded that they formed as 'primocrysts at the bottom of the liquid column'.

On the basis of the widespread development of size-zoned chadacryst populations in oikocrysts in the NTK intrusions, we conclude that much of the development of the picritic gabbrodolerite was predominantly by *in situ* nucleation and growth of a bed of crystals beneath flowing magma, rather than by transport and mechanical deposition of entrained olivine crystals. Further support for this model comes from the presence of dendritic crescumulate or harrisitic olivines in the intrusions (Fig. 13), further evidence for rapid *in situ* growth from transiently supercooled magma.

Could the silicate caps be anything other than segregation vesicles?

Segregation vesicles as originally defined by Smith (1967) are original gas-filled vesicles that have subsequently been infilled by products of silicate melt crystallization. Leaving aside for now the question of how this infilling happens, it is important to consider whether there are alternative explanations for the central key observation of this study: the association of sulphide globules with cavities, now filled by products of advanced fractional crystallization of intercumulus liquid, within the host cumulus crystal framework. The various alternatives are as follows:

1. The cavities are formed by original gas bubbles attached to sulphide droplets, this association being a consequence of the strong surface affinity between sulphide liquid and magmatic vapour (Mungall *et al.*, 2015).
2. The cavities were originally fully occupied by sulphide, whose volume has subsequently been reduced relative to the silicate framework cavity by (a) differential thermal contraction or (b) selective alteration and/or replacement.
3. The cavities were originally fully occupied by sulphide and the caps are generated by partial downward draining of the sulphide liquid into the surrounding pore space, forming the interstitial disseminated sulphide networks (Figs 4 and 8).

Considering the alternatives in reverse order, we first consider the extent of intercumulus sulphide percolation. It is clear from Fig. 1c–e that some 'leakage' of the globules has occurred into the immediately underlying intercumulus porosity. This is further investigated based on data from the high-resolution 3 D images (Figs

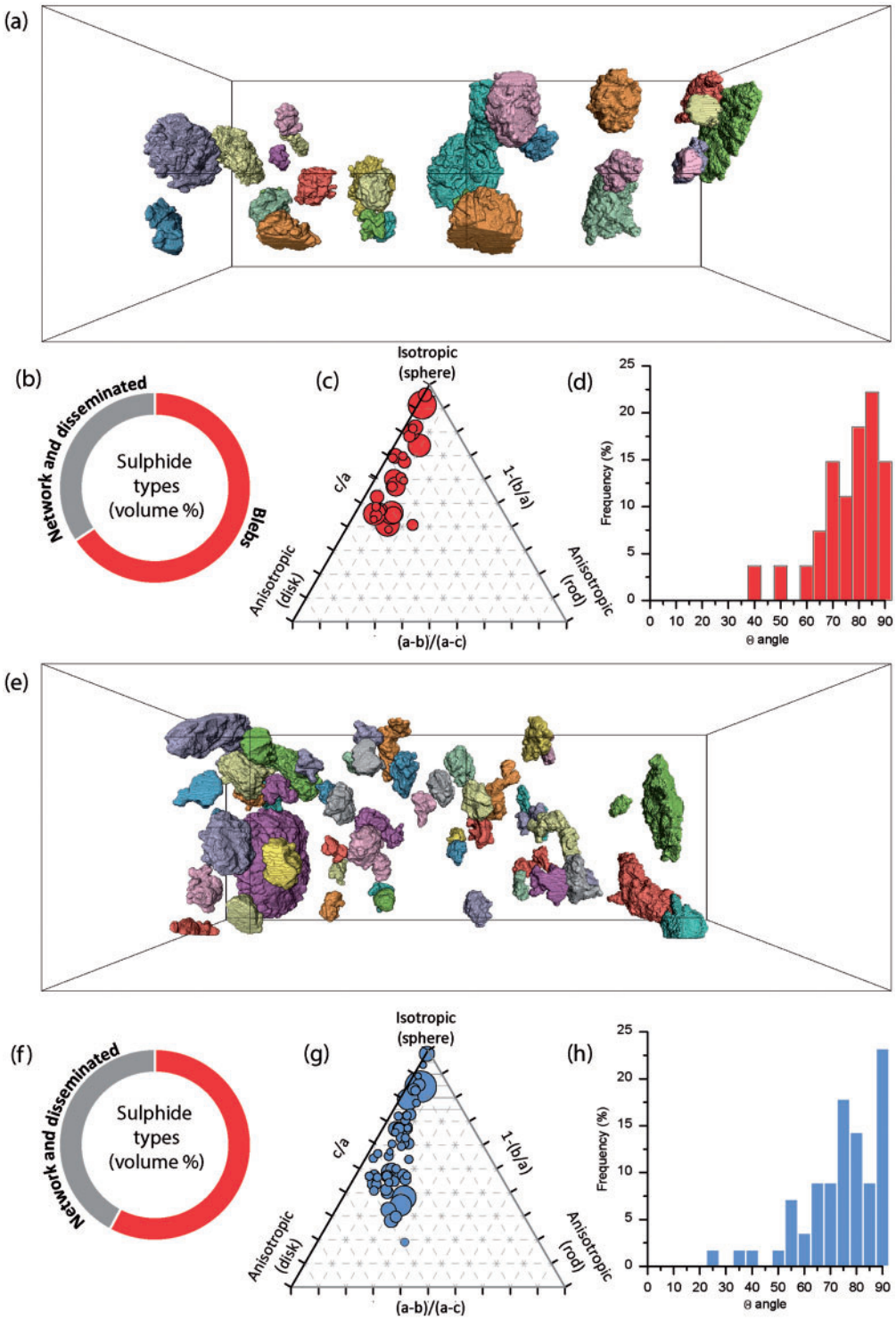

Fig. 10. 3D surface render of high resolution XRCT images of globules in samples VZU3 and RT7-147 (a, e) with interstitial network sulfides removed. (b), (f) indicate relative volume proportions of interstitial network sulphide to globular blebs. The orientation of the globules is represented on a shape discriminant plot (c, g) based on ratios of the principal axes of the best fit ellipsoid (a is the longest axis, c the shortest), with the size of the symbol proportional to the volume of the globule; note lack of systematic relationship between size and aspect ratio. (d, h) Orientation of each particle plotted as a histogram of poles to the plane of maximum flattening, relative to an arbitrary reference direction, showing strong shape-preferred orientation in both samples.

4 and 5). The high degree of interconnectivity of the fine interstitial sulphide is evidence that some percolation of sulphide melt through the pore space has occurred on a scale of at least several cm and possibly more. However, the interstitial sulphide component is present throughout the samples, both above and below the globules (Figs 4 and 5), and shows no evidence for having formed preferentially from downward drainage

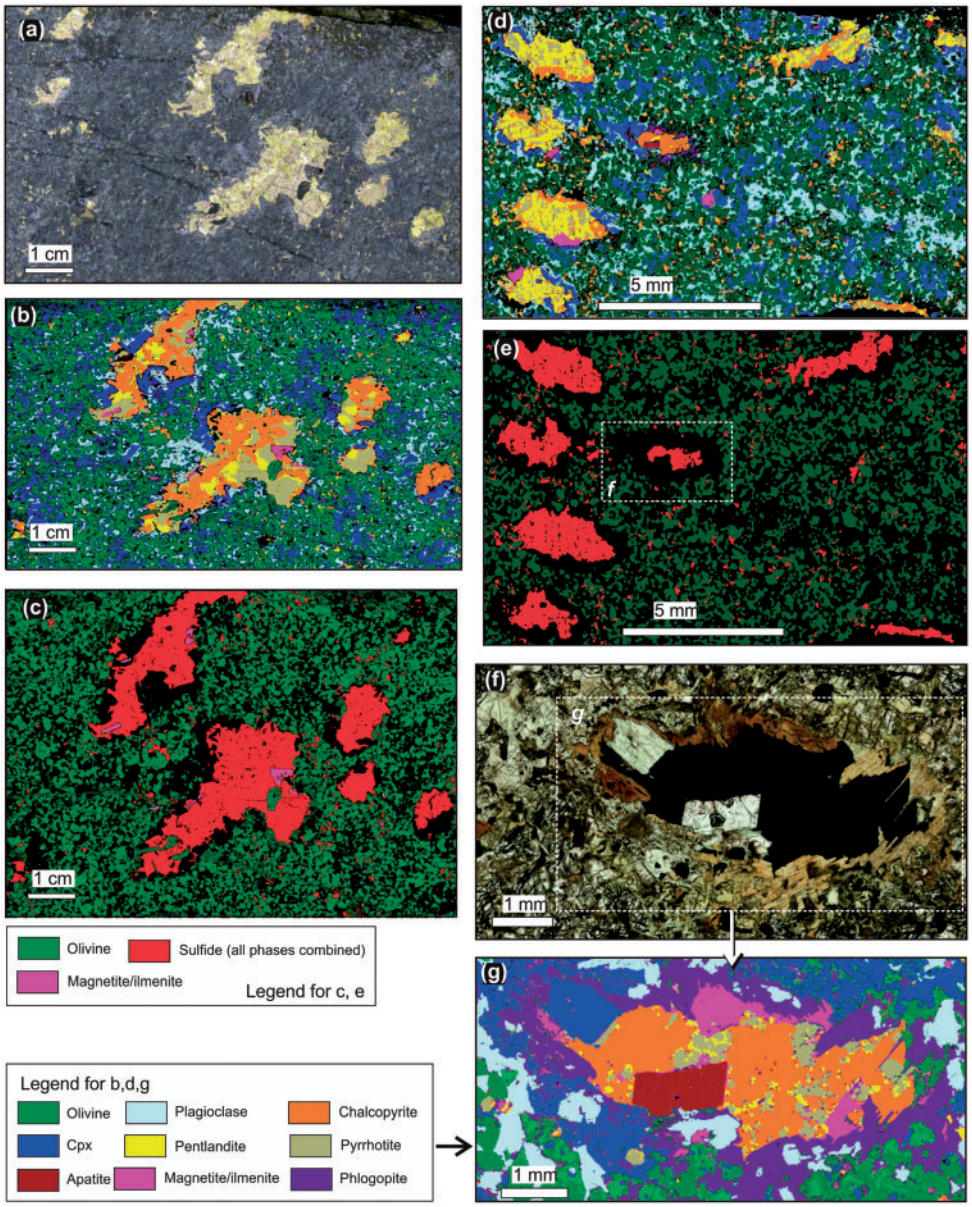

Fig. 11. Sulphide globules in picritic gabbrodolerites from the Kharealakh Intrusion, (a–c) samples VZU3 and (d–g) KH2. (a–c) Polished slab, Tornado-derived phase map and simplified sulfide-olivine-oxide phase map showing relationship of sulphides to olivine framework. (d, e) Same for sample KH2. (f, g) Transmitted light photomicrograph and phase map derived from SEM element mapping of detailed silicate cap area in (e).

from the underside of the capped globules, as would be necessary to account for the universal presence of the silicate caps above the globules. In most samples the relative volume of disseminated to globular sulphide (estimated in 3 D images where available and in the 2 D images otherwise, Table 1) falls between 13 and 32% of the total volume of sulphide in the sample, with mean values from 2 D images of 22%. In comparison, the proportion of silicate cap to globule volume, estimated from image analysis of 2 D sections, varies from around 30 to 100%; i.e. the volume of interstitial sulphide is not enough to account for the volume of the caps. Further, several samples show clear evidence of sub-solidus filling of amygdales by low-temperature minerals, clearly requiring the former presence of gas-filled voids. While downward percolation of the sulphide globules may have caused some further emptying of the cap space and drawing in of silicate melt, it is just as likely to have resulted in flow of sulphide liquid into the caps if no gas bubbles were present.

Most significantly, if the caps were formed purely by drainage, then infilling by silicate melt would be happening at the highest rate early in the solidification process where the porosity was highest. Consequently, there should be no systematic difference in mineralogy between the silicate caps and the remainder of the

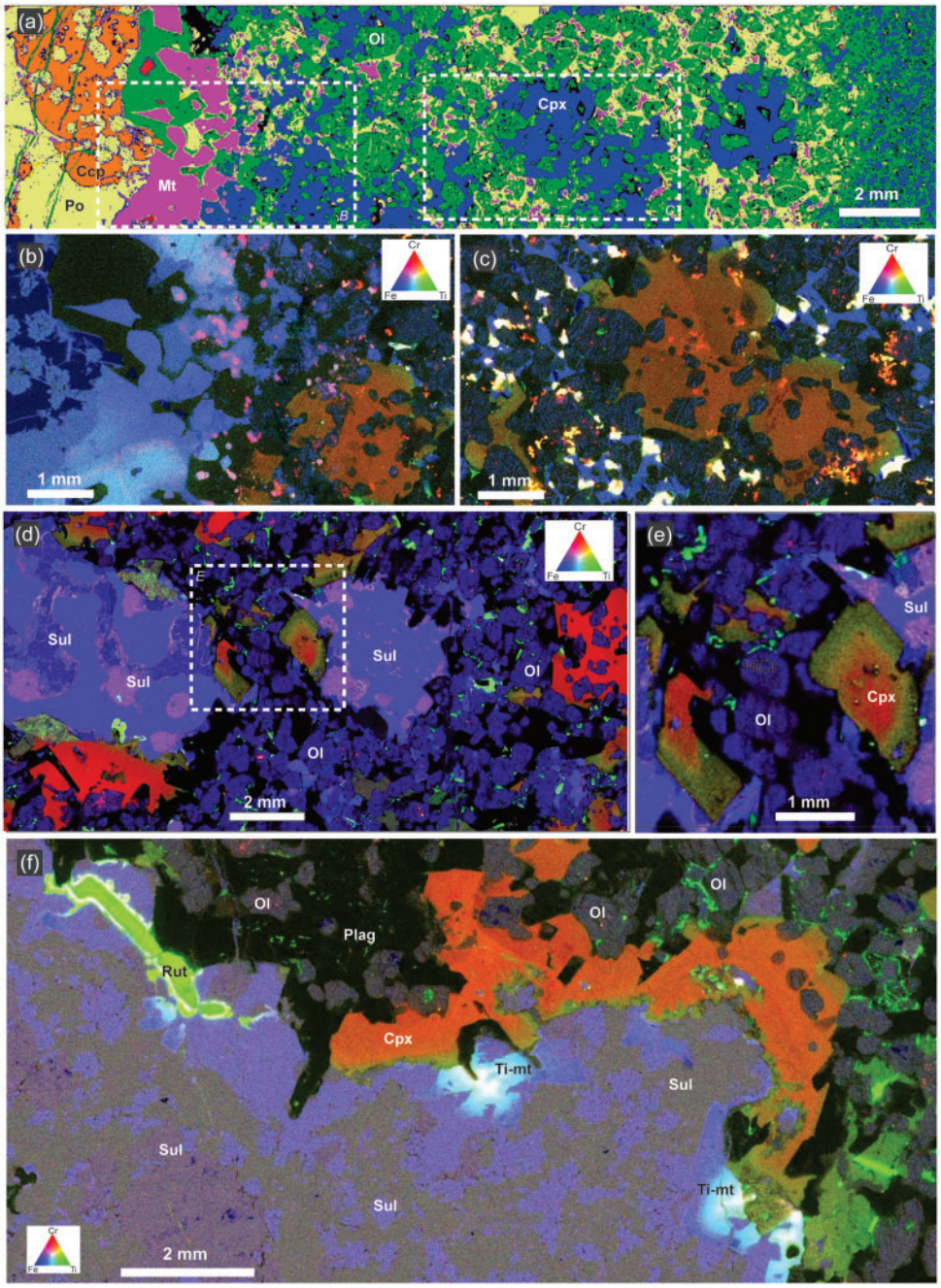

Fig. 12. (a–c) Samples ZF12-394 and (d–f)VZU3, phase map (a) and synchrotron Maia-XFM images (b–f) showing zoning in pyroxene and oxide phases associated with picritic gabbrodolerite matrix, sulphide margins and silicate caps (gaps between sulphide globules and the cumulus olivine framework). (a) Phase map; note relatively fine grain size of olivines enclosed within oikocrysts compared with those outside, and disseminated interstitial sulphide; fine grained material on far right is a xenolith. (b, c) XFM images of detailed areas (boxes in (a)) showing (b) chromite (pink) and zoned Fe–Ti oxides (shades of blue) at contact between sulphide and olivine framework; zoned cpx oikocrysts. (c) Prominent cpx oikocryst with sector zoning defined by variation in Cr content. (d) Sulphide moulded around zoned cpx, plag and Fe–Ti–Cr oxides. (e) Enlargement of cpx grains showing concentric zoning in Cr content (red) and outer faceted Ti-enriched zone (green). (f) Same relationship, note complex oxide mineralogy including rutile rimmed with Ti magnetite, and concentric zoning from Cr-rich to Cr-poor magnetite (white to blue), partially enclosed in sulphide.

intercumulus space. The predominance of highly differentiated residual phases in the caps (and not elsewhere) attests to migration of silicate melt down to the final stages of solidification and hence to the operation of gas filter pressing as discussed below. If the sulphide liquid had drained at a late stage, as suggested by Mungall (2002, 2007) at Sudbury, then there should be a compositional contrast between the intercumulus networks and the globules: the globules should be enriched in the solid product of differentiation of the sulphide liquid (MSS, enriched in Ni over Cu) relative to the percolating sulfide melt, which should be enriched

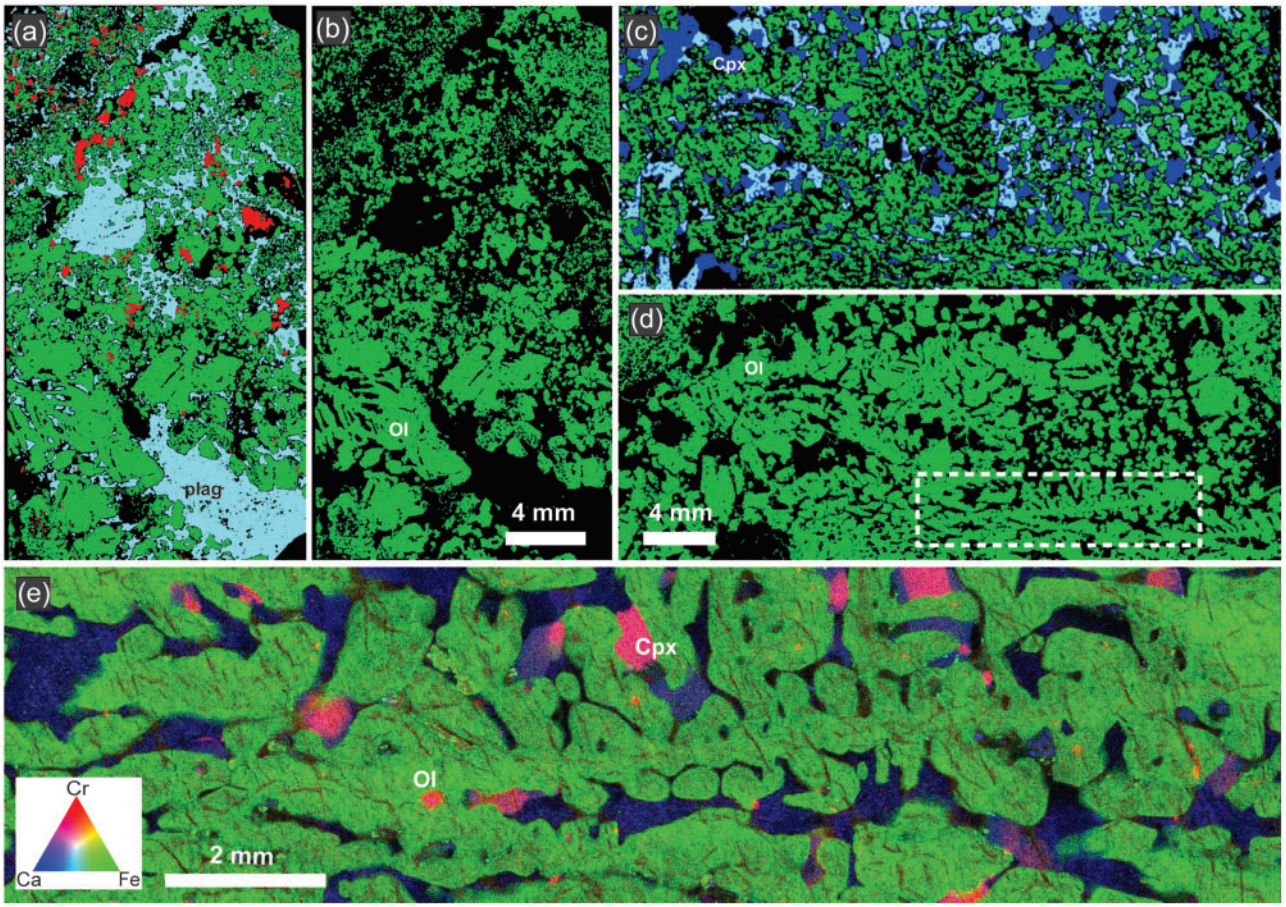

Fig. 13. Skeletal olivine grains from the Kharealakh intrusion. (a, b) Sample VZU7A, phase maps showing olivine, plagioclase (light blue) and sulfide (red) in a thin section. (c, d) Same, plus cpx (dark blue), sample ZF12-391.7. (e) same sample, detailed Maia XFM element map showing olivine single crystal (green) and zoned cpx (pink to blue); range in Cr_2O_3 contents from approx. 1–0·4%.

in residual liquid and hence in Cu over Ni. However, there is no discernible difference between the Cu/Ni ratio of the globules and intercumulus network sulphides (Le Vaillant, *et al.*, in preparation), indicating that sulphide percolation happened at an early stage before the sulfide liquid had started to solidify at about 1100°C, and hence before the generation of residual fractionated silicate melt which would be generated at temperatures close to the wet solidus, below 1000°C.

A final argument relates to the general rarity of the textures described here. Globular sulphide ores are not particularly common, but they are widespread in a wide variety of different nickel sulphide ore deposits, including several of the Sudbury deposits, Piaohechuan in China (Barnes *et al.*, 2017*b*), Nova-Bollinger in Western Australia and others. If silicate caps formed purely by drainage, then these textures should be ubiquitous in globular ores, whereas they are only observed in ores formed under low confining pressures where there is independent evidence of the presence of a free volatile phase during emplacement. We are, therefore, confident in concluding that the space now occupied by the silicate caps was not predominantly derived by partial drainage of the globules.

Differential thermal contraction offers a possible explanation for the caps, but the effect is extremely small. Pyrrhotite has a coefficient of thermal expansivity of approximately $8x10^{-5}$ (Tenailleau *et al.*, 2005) compared with values of around $3x10^{-5}$ for olivine-rich silicate rock (Afonso *et al.*, 2005). While sulphide droplets would be expected to contract more than the silicate framework, the expected relative volume change between sulphide and silicate over a 200°C melting range would be of the order of 1% (corresponding to a proportional change in radius of about 0·5%) much less than that required to form the caps. This effect can, therefore, be neglected.

Selective alteration has been noted for disseminated sulphides (Sluzhenikin *et al.*, 1994; Holwell *et al.*, 2017) and there is some evidence in the form of phlogopite penetrating into globules that could be taken as evidence of replacement. However, the characteristically smooth meniscus-like upper margin of many of the globules and generally pristine nature and magmatic mineralogy of most of the sulphide, contrasting with the pyrite, millerite, magnetite and carbonate assemblages typical of desulphidised magmatic ores (Barnes *et al.*, 2009), is not consistent with extensive replacement. Furthermore, replacement would be expected to

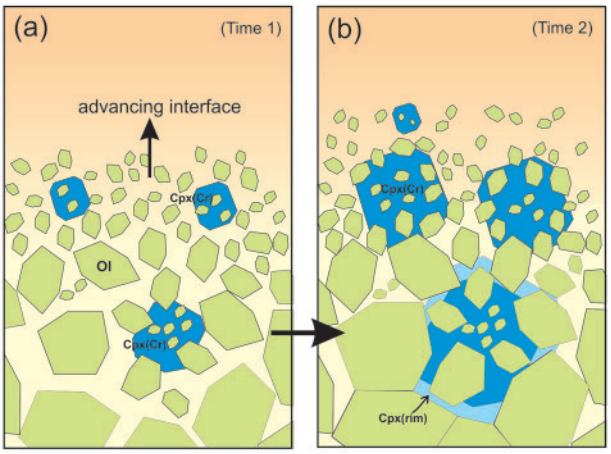

Fig. 14. Cartoon showing model for development of poikilitic textures by *in situ* growth at the top of a crystal mush layer. (a) Initial nucleation of olivine (green) and clinopyroxene (cpx, blue) from a melt saturated in olivine and supersaturated in pyroxene. Olivine grows slowly from abundant nucleii while Cr-rich cpx (Cpx-Cr) grows fast from sparse nucleii. (b) At a later stage cpx grains have overtaken growing olivine crystals, trapping smaller grains in the cores. Overgrowth from restricted melt volumes in the pore space within the mush forms Cr-poor, Ti-rich overgrowths, Cpx(rim).

progress inward concentrically from the margins of the sulphides, as in the examples documented by Holwell *et al.* (2017) and not just affect the upper margins in contact with the caps.

In the absence of plausible alternatives, we are confident in our conclusion that model 1 is the correct one and the silicate caps are segregation vesicles, i.e. formed by infilling of original gas-filled vesicles; in some cases, the original bubbles are still present in the form of amygdales, i.e. original gas bubbles now filled with low-temperature post-magmatic phases, within the silicate caps (Fig. 1g; see also fig. 1b of Le Vaillant *et al.*, 2017). This then raises two further questions: when did the vesicles form and should the sulphides be considered part of the filling of the segregation vesicle? Answering this question requires understanding of how the segregation process operates, but the question of timing needs to be considered first.

Accumulation model for sulphide globules and vapour bubbles

The Norilsk-Talnakh deposits contain unusually high proportions of the ores in the form of globular disseminated sulphides. Such ore types are present in many other deposits, but are more commonly a relatively minor component of the orebody as a whole. In some cases, such as globular ores at Sudbury, their composition and morphology suggests that they were derived by remobilisation of previously solidified sulphide liquid and were transported while partially solid (Barnes *et al.*, 2017*b*), whereas the globules at Norilsk must have been emplaced while molten to account for their highly consistent internal differentiation. The preferred interpretation of their prevalence at Norilsk is that globular ores are strongly favoured by the presence of a pervasive vapour phase, which in the case of the Norilsk ores is there for two reasons: extensive interaction with volatile-rich country rocks, recorded in the presence of xenoliths, taxites and contamination signatures (Arndt, 2011; Iacono-Marziano *et al.*, 2012, 2017); and the shallow depth and consequent low confining pressures accompanying emplacement.

A key question is whether the sulphide globules and gas bubbles were generated internally or transported in prior to crystallization of the silicates, or whether the degassing occurred within the crystal mush after accumulation of the sulphide droplets (Fig. 15). In the second alternative, interstitial vapour saturation in the mush during crystallization (commonly referred to as 'second boiling'), the association of sulphides with bubbles would be an *in situ* nucleation effect, whereas in the first it is the consequence of pre-cumulus vapour saturation ('first boiling'). i.e. the bubble-rafting process identified by Mungall *et al.* (2015). Both are capillary wetting effects, driven primarily by preferential nucleation of vapour bubbles on sulphide liquid due to surface energy effects. The distinction in timing is of potentially great significance in understanding ore forming processes in these supergiant deposits.

Bubble nucleation in the mush by second boiling could be driven by either or both of two main processes: reduction in confining pressure during eruptions (discussed further below), or driving of volatile-enriched magma towards volatile saturation during progressive crystallization. However, several arguments can be made against second boiling in this case. In the presence of a cumulus sulphide liquid phase, nucleation of bubbles would be achievable at very low degrees of supersaturation, owing to the wetting tendency of vapour against sulphide (Mungall, 2015). Hence gas bubbles would nucleate uniformly wherever there was sulphide. In the Norilsk picritic dolerites, patches of interstitial disseminated sulphide without bubbles are common, whereas bubbles are consistently found associated with the subspherical globules and not uniformly throughout the sulphide-bearing domains in the rock. Larger bubbles are generally attached to larger droplets, which implies they arrived together. Bubbles are always at the tops of globules, but would also be expected to be associated with the interstitial sulphide component if they nucleated in the mush, where they should nucleate randomly wherever there is any sulphide. Many globules lack bubbles altogether. The olivine framework is homogeneous and isotropic; there is no sign of deformation or change in the nature of clustering or packing around the bubbles, which would be expected if the bubbles and sulphides were migrating through the mush to produce globules, or if large bubbles were growing in the mush and pushing aside olivine crystals. There is no evidence for the presence of vesicles or amygdales in the picritic gabbrodolerites in the absence of sulphides.

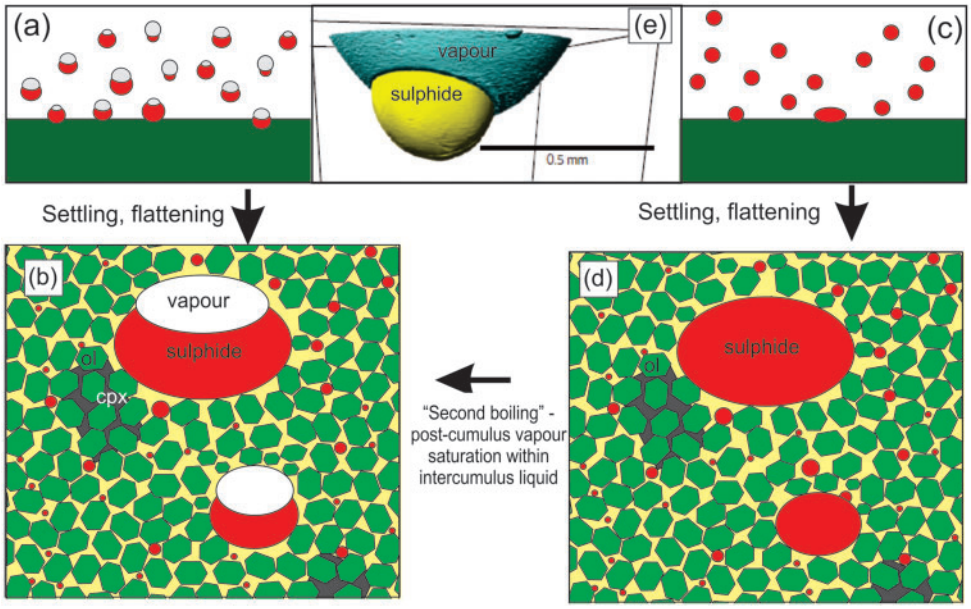

Fig. 15. 'Bubble riding' or *in situ* vapour saturation? Alternative scenarios for development of globule–bubble associations in the cumulates. Path 1 (a, b) involves accumulation of composite globule–bubble pairs into crystal pile, with flattening due to balance between weight of globule and surface tension force. Option 2 (c–d; b) accumulation of vapour-free sulfide globule, followed by vapour-phase saturation of interstitial liquid and nucleation of bubbles on previously accumulated globules. (Relative size of gas bubble exaggerated for clarity). (e) 3D image from x-ray microtomography of a composite sulfide (yellow)–vapour (blue) droplet–bubble pair from an experimental run (Mungall *et al.*, 2015).

An important line of evidence is in the flattening of the droplet–bubble composites (Figs 1 and 15). This feature could be produced either by compaction of the crystal mush with embedded globules, or by flattening of the droplets under their own weight as they accumulated at the top of the crystal pile. The textures of the olivine cumulates show no evidence of wholesale compaction, and the early crystallization of oikocrysts, argued for above, implies that the crystal pile behaved as a rigid framework from an early stage as it developed. There is no sign of deformation of the olivine framework around the oikocrysts, as would be expected if the cumulate pile had compacted. The flattening of the droplets is, therefore, likely to be a gravitational sessile drop effect. The fact that the silicate caps follow the morphology of the droplets implies that they were present at the same time as the arrival and gravitational deformation of the settled droplet. We can, therefore, conclude that the sulphide globules were transported and deposited while attached to gas bubbles: they formed by first boiling, not second boiling.

Vesiculation in the sub-surface is likely to be related to simultaneous eruptive activity above. Pyroclastic eruptions are interspersed with the overlying and demonstrably coeval Mokulaevsky suite lavas (Sluzhenikin *et al.*, 2014). Their presence implies either periodic volatile oversaturation in the underlying plumbing system, or episodic interaction of the shallow magma reservoir with ground water, or a combination of the two. In either case, explosive venting of magma to the surface would be accompanied by rapid transitions between the limits of lithostatic and hydrostatic pressure. Such fluctuations could also explain the subsequent infilling of the vapour caps, to which we now turn.

How do segregation vesicles fill with melt?

The mechanism of formation of segregation vesicles was first considered by Smith (1967), who was also the first to recognise the phenomenon and coin the terminology. Smith considered a number of options, including the simplest hypothesis that gas law behaviour would cause shrinking of the gas volume in the vesicle with cooling over the melting range of the basalt. If the lava had solidified just enough to form a rigid framework of touching crystals, then this contraction should draw residual liquid into the vesicles. However, Smith pointed out that the total volume reduction over the melting range of the basalt would be very small, around 15%, compared with the 50% or more infilling observed in the basalt flows which he studied. Therefore he proposed that additional shrinkage of the gas volume was caused by flowage of the lava into deeper water, resulting in an increase in confining pressure and shrinkage of the gas bubbles. However, this requires that the lava would fall into a narrow window of rheology in which the crystal framework was rigid enough to preserve the original walls of the vesicle, but the lava was still able to flow.

An alternative mechanism, gas filter pressing, was proposed by Anderson *et al.* (1984) and has since become widely accepted as a mechanism to form not only segregation vesicles in lava flows and dykes (Sanders, 1986; Merle *et al.*, 2005) but also veins and sheets of segregated fractionated melt in basaltic lavas (Martin &

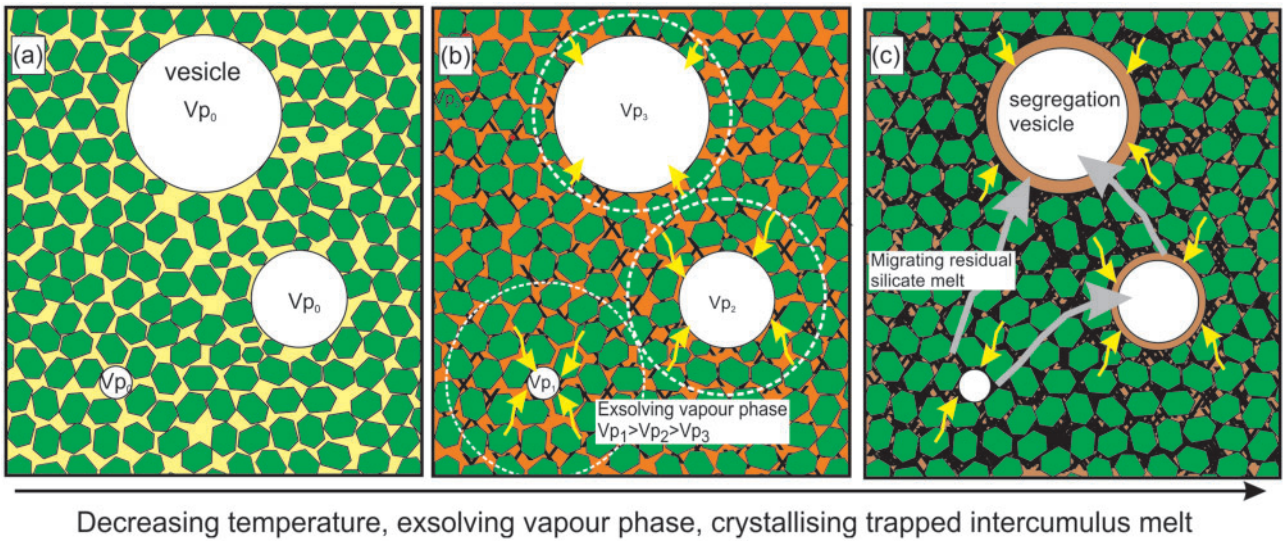

Fig. 16. Simplified representation of the Anderson *et al.* (1984) mechanism for formation of segregation vesicles by gas filter pressing. (a) Temperature 1 (highest), vesicles of variable size are held within a rigid framework of partially crystalline mush; vapour pressure Vp_0 initially the same in all the vesicles. (b) Temperature drops, causing crystallization of a proportion of the vapour-saturated interstitial liquid in the mush (forming intercumulus phases shown in black), releasing additional vapour (yellow arrows) by second boiling. Considering the mass of additional vapour released within a given volume of mush represented by the dashed white circles, the mass proportion of this additional vapour to the vapour in the original bubble is highest around the smallest vesicles, hence the vapour pressure Vp is increased by a larger amount in the smaller vesicles than in the larger ones, such that $Vp_1>Vp_2>Vp_3$. (c) Ongoing crystallization and vapour exsolution, residual trapped liquid (brown) migrates along pressure gradients within the mush to line the original vesicles, forming segregation vesicles.

Sigmarsson, 2007; Sigmarsson *et al.*, 2009). As in the Smith model, the mechanism also requires that crystallization of a volatile-saturated melt proceeds to the point at which the walls of the original gas filled vesicles become rigid while interstitial melt is still present. As crystallization proceeds and second boiling progressively releases exsolved vapour into the residual porosity, pressure in the voids (vesicles, or diktytaxitic pores) increases (Fig. 16). The key element of the model is that pressure in the smaller voids builds up more rapidly than in the larger voids, generating pressure gradients that progressively drive more and more fractionated melt into what remains of the pore space. Anderson *et al*'s (1984) calculations show that pressure differentials of the order of several bars can develop on a scale of mm between adjacent voids. Eventually, the most fractionated melt ends up in the last remaining voids, which were the largest original vesicles. This mechanism can cause up to 70% filling of the original vesicle space.

The appeal of the gas filter pressing mechanism to explain the Norilsk segregation vesicles is obvious. The Ti-rich mineralogy and mineral zoning patterns documented within the segregation vesicles associated with the sulphide globules clearly represent the crystallization of highly fractionated residual liquid, derived from advanced crystallization of the trapped intercumulus melt component, exactly as predicted by the Anderson model. A model based solely on externally imposed pressure increase without gas filter pressing can explain migration of melt into the original bubble space, but not that this in-filling melt has a highly-fractionated composition.

Gas filter pressing solves the problem of near-filling of the vesicles and the composition of the infilling phases. However, the process depends critically on the relative timescales for: (a) migration of the trapped melt through the residual porosity; (b) diffusion of volatiles through the melt; and (c) the solidification process that generates the pressure gradients. Primarily, crystallization has to be proceeding fast enough that pressure gradients are maintained against the tendency of water diffusion through the melt to even them out (Mungall, 2015). Anderson *et al.* (1984) demonstrated that the latter condition is likely to hold for rapidly cooling lava flows, but Mungall (2015) argues that dissipation of pressure gradients by diffusion will dominate in plutonic settings. Further, it is necessary for pressure-driven Darcy flow of the residual interstitial melt through the residual pore space to operate on a shorter timescale than water diffusion. Resolution of this condition requires rigorous evaluation, beyond the scope of this study, but we argue on the evidence presented here that the shallow Norilsk ore-bearing intrusions crystallized at faster rates than those considered by Mungall (2015), such that gas filter pressing was able to operate.

Some problems remain. Firstly, the Anderson model predicts maximum infilling of the largest vesicles to about 70%, whereas the examples described here in many cases appear to have filled almost completely with segregated fractionated melt. Secondly, the exact relationship of the sulphides to the morphology of the vesicles remains puzzling.

In the Mungall *et al.* (2015) 'bubble-riding' scenario, the balance of surface tension and gravitational forces

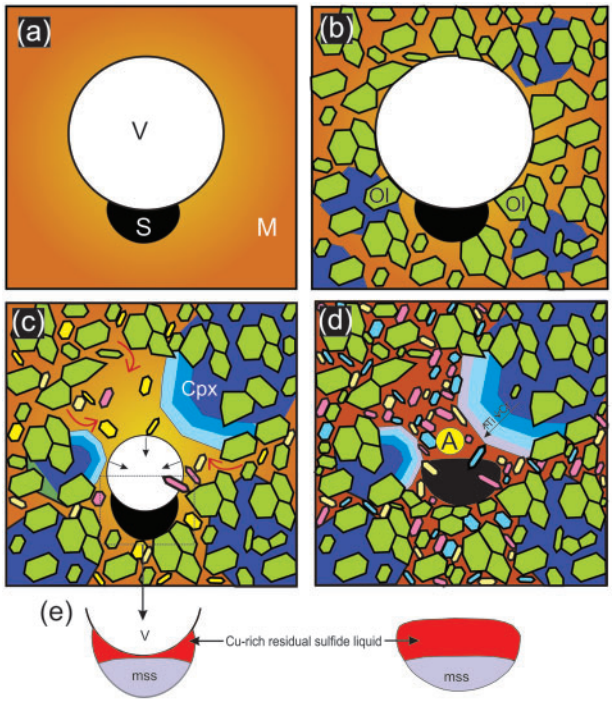

Fig. 17. Cartoon of pressure increase–bubble contraction model. (a) Droplet–bubble pair suspended in carrier magma. (b) Accumulation in crystal mush, development of rigid cumulus crystal framework. (c) Increase in confining pressure causes decrease in volume of vapour bubble while leaving walls of intercumulus cavity unmodified, causing silicate melt to migrate into the cavity. Simultaneously the sulphide globule begins to crystallize, forming MSS and residual liquid that maintains contact with the residual vapour bubble. (d) Ongoing droplet contraction, coupled with gas filter pressing driving highly fractionated silicate melt components into the residual pore space; differentiation of sulphide liquid globule continues to final solidification, moulding around pre-existing accessory oxide/silicate/apatite phases (Pink/yellow). V, vapour; A, amygdale; Ol, olivine; S, sulphide melt; M, silicate magma.

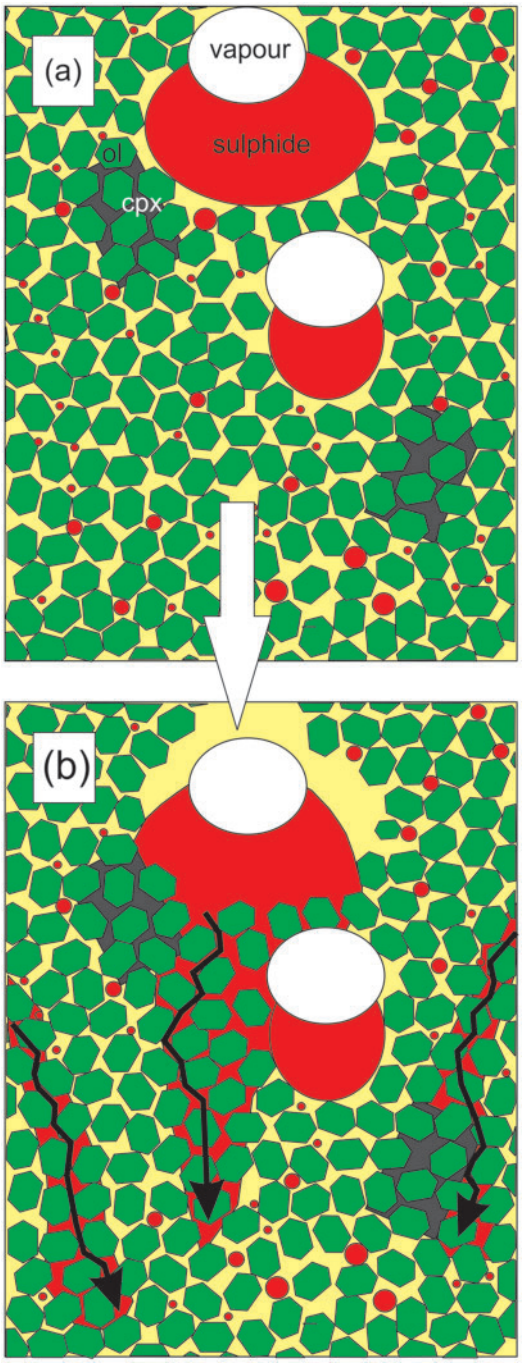

Fig. 18. Percolation model based closely on that of Barnes *et al.* (2017b). (a) An initial population of globule–bubble pairs and small stranded droplets evolves towards a population of droplet–bubbles, stranded droplets and interconnected network sulphides derived by gravity-driven percolation of those few globules large enough to exceed the critical percolation threshold. These networks locally engulf the stranded globules and droplets giving rise to the observed texture (b).

dictates that the meniscus between the gas bubble and the sulphide droplet be convex downward, i.e. into the sulphide, as observed in experiments (Fig. 15). However, in the natural examples described here, the meniscus is always reversed, i.e. convex up into the bubble. This indicates that the final configuration of the bounding meniscus of the sulphide droplet is not with the gas bubble, but rather with silicate melt. A plausible mechanism for this is for the gas bubble to shrink within its rigid container, i.e. the space in the cumulus framework occupied by the original gas bubble–droplet pair, as a result of an increase in the confining pressure, as in the original Smith model. Therefore we propose that a combination of increased confining pressure and Anderson gas filter pressing operated during solidification of these cumulates, resulting in near complete infilling of the original vesicle with strongly fractionated silicate melt (Fig. 17). The driving pressure increase could have been due to progressive accumulation of the overlying basalt lava pile, or more likely due to a restoration of lithostatic pressure following sealing of water filled cracks, generated during explosive volcanic episodes that perhaps drove the vesiculation in the first place. Neither the Smith compression nor the Anderson gas filter pressing model can fully explain the observations, but the operation of both together can explain both the meniscus shape problem and the highly

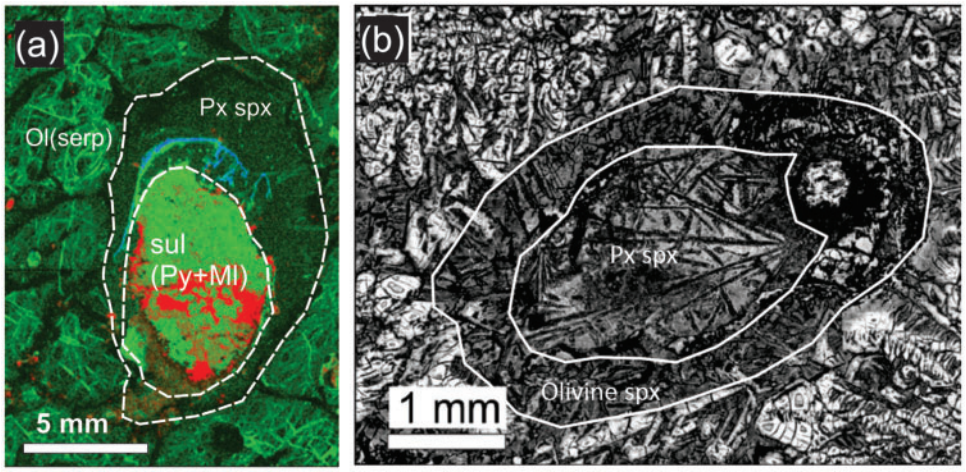

Fig. 19. Segregation vesicles in komatiitic cumulates. (a) Black Swan, globular sulfide (now altered to millerite, pyrite, carbonate) with skeletal chromite rind enclosed within pyroxene spinifex filled segregation vesicle in harrisitic olivine orthocumulate. (b) Murphy Well segregation vesicle, showing outer zone of olivine spinifex textured komatiite melt, lined with inner zone of pyroxene spinifex, and residual amygdale in upper right.

fractionated nature of the cap contents. Further, the Anderson mechanism gives us an explanation for the otherwise perplexing internal differentiation of the globules, as discussed further below.

Bubble and sulphide melt dynamics in crystal mushes

Mungall (2015) presents an exhaustive analysis of the physics of bubble nucleation, growth and migration (or otherwise) in solidifying crystal mushes. Bubbles can occupy three distinct regimes: (1) microbubbles, which are smaller than the intercumulus pore throats and capable of migrating upwards under buoyancy through the pores; (2) stranded bubbles, which occupy pore chambers (spaces between four or more grains), but are prevented by capillary forces from migrating through pore throats; and (3) extended bubbles, which are larger than pore chambers, but have sufficient rise height and consequent buoyancy to overcome capillary forces and essentially squeeze themselves upwards through the pore space. Almost exactly the same principle, with the buoyancy force reversed to act down rather than up, applies to sulphide droplets (Chung & Mungall, 2009; Barnes *et al.*, 2017*b*). Mungall (2015) concluded that vapour bubbles are typically unable to migrate upward through crystal mushes and hence would primarily remain 'stranded', as we observe. The samples studied here represent a very rare example in which we can observe the effects of all these processes in a natural system.

The condition for transitioning from stranded to extended bubbles, like that for stranded droplets to migrating sulphide networks, depends primarily on the grain size of the cumulus framework. Taking an estimate of 1 mm for the characteristic olivine grain size in the picritic gabbrodolerites, based on Mungall's (2015) calculations vertical bubble extents of between 50 and 120 mm would be necessary to enable migration of extended bubbles, neglecting the opposing force due to the capillary attraction between the vapour bubbles and the sulphide droplets. The largest bubbles we observe have diameters of the order of 10 mm, such that no migration would be expected. All of the bubbles, except possibly the smallest, would fall within the 'stranded' regime.

The same is true for the sulphide globules. Again, leaving aside the effect of capillary attraction to the bubbles, we can compare the characteristic size range of the globules to the exactly equivalent regime boundaries derived by Chung & Mungall (2009). For olivine grains of 0·5 and 1 mm and olivine proportion of 60%, the threshold for sulphide percolation is a rise height (equivalent to globule radius) of 120 to 150 mm, well above the range of globule sizes. Most of the sulphide globules would not be expected to percolate. Nonetheless, we note that in many cases the globules are connected to larger interconnected, disseminated sulphide networks (Fig. 8) on a scale of several cm (the estimate being limited by the size of the scanned sample). It appears, therefore, that while most of the globules remained effectively stranded in the crystal framework, originally larger ones were able to overcome the capillary resistance and percolate downward, collecting up other stranded droplets as they went to form larger mobile networks (Figs 8 and 18). The percolating networks must have started as unusually large globules, possibly formed by post-accumulation coalescence, and/or developed early when the porosity of the cumulate network was higher. A component of the network sulfide may also have formed by coalescence of fine droplets small enough to pass through intercumulus pore throats (Chung & Mungall 2009).

The co-occurrence of globular and interstitial disseminated sulphides in the same rock is unusual, but not unique. Other examples have been reported by Barnes *et al.* (2017*b*) from komatiite-hosted deposits at Alexo

(Abitibi Belt, Canada) and Mesamax (Cape Smith belt, Canada) and by Godel *et al.* (2013*a*) at Mt Keith, although silicate caps are lacking in the latter two examples. In these cases, the interstitial disseminated component is thought on the basis of 3D tomography evidence to have formed by percolation of critical-sized sulphide networks from above (Barnes *et al.*, 2017*a*) into an orthocumulate already containing stranded globules, as in the interpretation offered here and illustrated in Fig. 18.

Other examples of segregation vesicles in cumulates

Sulphides associated with vapour bubbles have been reported in a number of komatiitic bodies (Keele & Nickel, 1974; Eckstrand & Williamson, 1985; Stone *et al.*, 1996; Beresford *et al.*, 2000; Barnes *et al.*, 2009). The most closely analogous example is reported from komatiitic cumulates from the Black Swan area, Western Australia (Barnes *et al.*, 2009). In this case, (Fig. 19a) the geometry of the structures is very similar to that reported here; sulphide forms globules enclosed within subspherical voids in the cumulate framework, with the silicate cap being filled by alteration products of pyroxene spinifex-textured quenched komatiite melt. In the Black Swan case, an externally imposed pressure increase is also a plausible model, in that the globules formed within an upward accreting thick cumulus pile in an inflating komatiitic flow channel (Hill *et al.*, 2004).

An example of the filling of segregation vesicles with progressively more fractionated melt is seen in a sample of an unusual vesicular komatiite from the Murphy Well flow in Western Australia (Siégel *et al.*, 2014) (Fig. 19b). In this example, the outer part of a segregation vesicle is lined with more primitive liquid, crystallising to olivine microspinifex plates, while the inner zone is lined with pyroxene microspinifex needles. Clearly the migrating pore liquid was evolving while the vesicle was filling, as seen in the Norilsk-Talnakh samples.

Other examples of capped globules dispersed within dolerite dykes have been described from East Greenland (Holwell *et al.*, 2012) and from Uruguay (Prichard *et al.*, 2004). Both of these occurrences are clear examples of the type of bubble–droplet association reported here. In the case of the East Greenland example, the sulphide liquid appears to have been derived by assimilation of sulphide at a higher crustal level than the position at which it froze into the dyke margin (Holwell *et al.*, 2012) indicating that the droplet–bubble pairs were negatively buoyant and sank. The process of sulphide liquid transport mediated by bubble attachment may be widespread in shallow level systems.

Role of vapour phase in sulphide differentiation

Strong internal differentiation of sulphide globules into Cu-rich upper zones and Cu-poor, Ni-rich lower zones, with smooth menisci between them, is a hallmark of the globular ores in the Norilsk picritic gabbrodolerites, but has also been noted elsewhere: in margins of macrodykes in East Greenland (Holwell *et al.*, 2012), in dolerite dykes from the Uruguay swarm (Prichard *et al.*, 2004) and in the sub-volcanic Insizwa Complex in Natal (Lightfoot & Naldrett, 1984); in all of these cases the sulphides are associated with silicate caps. In globular ores lacking silicate caps, as at Sudbury, the globules typically lack the strong gravitationally-controlled internal differentiation characteristic of the Norilsk-Talnakh globules (Barnes *et al.*, 2017*b*).

The conventional sulphide liquid differentiation model for the Norilsk globules (Barnes Sarah *et al.*, 2006) require that the solid 'cumulus' MSS component sinks to the bottom of the droplets while the residual Cu-rich liquid rises to the top. However, this is unlikely to have happened for a number of reasons. The density difference between the two phases is likely to be very small and, if anything, the Cu-rich phase is likely to be slightly denser (Kress *et al.*, 2008); even if the solid phase were denser, at the very small length scales operating within individual globules, surface forces are likely to be dominant over gravity, such that gravitational separation would be inoperative. The textural relationship of pyrrhotite and pentlandite to the enclosing crystal framework is a key piece of evidence here, particularly the moulding of large single MSS crystals around idiomorphic grains of apatite and Ti-oxides noted above. Crystallization of apatite and Ti-rich phases directly from the sulfide liquid is highly unlikely due to the non-chalcophile character of the components Ca, P and Ti; this relationship, therefore, proves that the MSS grew around the silicate minerals, rather than settling from the liquid globule.

The gas filter pressing model, coupled with the surface affinity of sulphide liquid with vapour, provides an explanation. The solidification range of the sulphide liquid would have been in the range of 1100–800°C, broadly similar to that of the volatile-enriched mafic silicate melt (Kullerud *et al.*, 1969; Hill, 1984). Hence, the sulphide liquid was crystallising while the silicate melt was migrating into the adjacent vesicles. Adherence between the vapour phase and the residual Cu-rich liquid would have continued to draw that liquid into the vesicle space and to the top of the solidifying sulphide mass; sulphide liquid differentiation, as well as silicate liquid differentiation, was accentuated by gas filter pressing.

Model for formation of globular sulphides within segregation vesicles

From the lines of evidence presented here we conclude that a component of the Norilsk-Talnakh sulphide globules was transported and deposited as compound droplet–bubble pairs (Fig. 15a and b) generating gas and sulphide filled cavities within the framework of cumulus silicates, itself generated largely by *in situ* nucleation and growth at the floor of the magma conduits. In our

proposed model, vapour phase saturation was favoured by assimilation of volatile-rich sediments, including carbonates and sulphates (Arndt, 2011; Iacono-Marziano *et al.*, 2012). Bursts of vesiculation may have been generated during transient pressure drops associated with eruptions. Subsequent pressure increase, either due to crack sealing or gradual accumulation of overlying basalt flows, caused the gas bubbles in the cavities to contract, drawing progressively evolving residual silicate melt into the cavities (Fig. 17). Hence the final morphology of the sulphide melt is controlled by the sulphide-liquid melt meniscus, rather than by the original sulphide-vapour surface. Ongoing gas filter pressing continued to drive silicate melt into the residual pore space, while also driving physical segregation of residual Cu-rich melt from the differentiating sulphide globules into the cavity above, thus explaining the remarkably complete separation of sulphide phases at a scale at which surface capillary forces would be expected to be dominant over gravity.

Taking a broader view of the mineral system as a magma transfer network, we can speculate about possible transport and deposition mechanisms. The ore-bearing intrusions form part of a vertically extensive sill–dyke complex (Barnes *et al.*, 2016*b*), containing a cloud of finely dispersed sulphide droplets generated by incorporation of S from anhydrite and other sedimentary components. Much of this sulphide may have been generated near the top of the sill–dyke column at or near the level of the Norilsk 1 intrusion, as a result of assimilation of coal and reduction of oxidised sulphate-bearing magma that had assimilated anhydrite at greater depths (Naldrett, 2004; Iacono-Marziano *et al.*, 2017). Hypothetically, the pressure drops suddenly during eruptions and a cloud of bubbles forms. These bubbles nucleate preferentially on sulphide droplets, owing to the strong effect of wetting on reducing the activation energy for nucleation of the vapour phase (Mungall, 2015). The buoyancy of the composite droplet–bubble pairs would depend on the relative proportions of both phases: taking sulphide liquid density as 4400 and silicate liquid as 2600 kg m^{-3}, a volume ratio of 1·4:1 of sulphide to vapour (i.e. a gas bubble 70% of the volume of the droplet) would produce a droplet–bubble pair with neutral buoyancy in basaltic melt. Pairs with more gas would float and those with less gas would sink (see Lesher, 2017; Yao et al., unpublished data). As the positively or neutrally buoyant population is carried up by ascending magma, the decreasing pressure causes an increase in bubble size and increased buoyancy of the bubble–droplet pairs, a self-reinforcing process which could cause a champagne cork surge of bubble-riding sulphide into the upper portions of the system and potentially into the atmosphere (Le Vaillant *et al.*, 2017). At the end of eruption stages, pressure returns to fully lithostatic, the bubbles contract, and the direction of motion reverses for those originally buoyant pairs still within the magma column. The droplets with less sulphide and more vapour would tend to be carried out of the system altogether as eruption products, while those with more sulphide and less vapour would tend to settle and accumulate, to form the orebodies or other accumulations below the limits of exploration. The globules preserved within the orebodies would obviously have to be those that had negative buoyancy and settled into the cumulate layers. As the denser droplet–bubble pairs still within the magma column settle, increased pressure would cause the bubbles to contract, further increasing the density. Larger droplets with small or absent bubbles would tend to break up under their own weight into smaller droplets as they settled (Robertson *et al.*, 2015), accounting for the scarcity of globules greater than about 2 cm in size. Deeper sulphide accumulations might be tapped and re-entrained during subsequent pulses of magma upflow, recharge and eruption. In this way, prolonged recycling and upward and downward migration of bubble-associated sulphide liquid droplets, in a kind of large-scale magmatic elutriation column, could overcome some of the kinetic and mass-balance difficulties associated with generating large volumes of high-R factor sulphides (Barnes & Robertson, 2018).

We emphasize here that we are not implying that buoyant 'bubble-rafting' was the predominant mechanism of ore formation in the Norilsk-Talnakh intrusions. As noted in the descriptions, many globules do not have silicate caps and many that do would still be expected to be denser than the carrier magma, as pointed out by Krivolutskaya *et al.* (2018*b*). Much of the transport of sulphide droplets was most likely by normal processes of entrainment in flowing magma. However, bubble rafting may provide a solution to one of the many enigmas of these deposits: the presence of large volumes of sulphide droplets of a size that would be expected to break up and disperse into much finer droplets under their own weight in the carrier magma during transport (Robertson *et al.*, 2015).

A major unsolved paradox remains: where are the erupted equivalents of the sulphide-bearing, strongly PGE-enriched sulphide suspensions with heavy S isotopic compositions that formed the orebodies? The presence of large tonnages of sulphide ores in the Norilsk 1 intrusion, emplaced into the base of the basalt pile above the uppermost evaporate strata, proves that some sulphides must have been transported upward at least short distances, but eruptive equivalents are either absent, or have not yet been sampled. There are at least three possible explanations:

1. The number of sulphide–bubble pairs that were erupted is far less than the number that were deposited. This explains the high enrichments of PGE in the ores and the absence of complementary sulphide or PGE enrichment in the lavas (see Lesher, 2017; Lesher, *in press*). In this case, the enormous amounts of S and Ni that have been envisioned to have been released (Rothman *et al.*, 2014; Le Vaillant *et al.*, 2017; Rampino *et al.*, 2017) came from the

Siberian LIP as a whole and not exclusively from the ore-forming system.
2. The products resulting from the eruption of sulphide–bubble pairs are represented by pyroclastic rocks rather than massive lavas and consequently might not be reflected in the existing geochemical data sets on the lavas.
3. The ore-bearing intrusions are blind to the surface (Krivolutskaya, 2018*b*), and either the notion of ore formation in flow-through conduits is incorrect, or (more likely in our view) the magmas that formed the orebodies are now preserved in distal flanking sills that have yet to be sampled. Extensive sill complexes in large igneous provinces (LIPs), such as the Siberian LIP, have been shown to extend laterally for 1000s of km, and may be emplaced primarily as interconnected stepped sills (Magee et al., 2016*a*, 2016*b*) without necessarily feeding overlying volcanism, consistent with the relationships shown by Krivolutskaya (2018*b*).

Resolution of this paradox is beyond the scope of this study, but presents a significant challenge to ongoing research on these orebodies.

CONCLUDING COMMENTS

The distinctive differentiated globular sulphide ores of the Norilsk-Talnakh camp have textures indicative of accumulation of sulphide globules attached at the cumulus stage to vapour bubbles; these bubbles are now preserved as partially or completely infilled segregation vesicles within predominantly olivine orthocumulates. The presence of a highly fractionated, silicate–oxide component in the segregation vesicles, as well as the highly regular internal differentiation of the globules with Cu-rich residual melt products at the top, is attributed to an interplay between two processes: shrinking of the gas bubbles due to increase in confining pressure, and gas filter pressing partially filling the residual space with residual silicate and sulphide melt. The presence of an interconnected interstitial sulphide network in some samples is attributed to downward percolation of critical-sized sulphide blebs from above, into orthocumulates already containing globular sulphide droplets.

We suggest that the effect of 'bubble-rafting' of sulfide globules may play a significant role in the transport and deposition of the Norilsk-Talnakh ores, but we emphasize that this is largely speculation subject to better understanding of the dynamics of the process. A significant limit may be the maximum sizes of bubbles and droplets that can remain attached to one another, the physics of this being beyond the scope of this contribution.

The Norilsk-Talnakh camp is remarkable in many ways, in addition to its exceptional size and wealth of endowment. The observations reported here suggest that an important contributor to its uniqueness is its shallow depth of emplacement, coupled with the availability of abundant volatile components through sediment assimilation. One of a number of enigmatic features is the apparent lack of erupted lavas with compositions consistent with the observed olivine-rich mineralogy and isotopic composition of the ore bearing intrusions (Latypov, 2002; Ripley *et al.*, 2003; Krivolutskaya, 2011) and the absence of coeval lavas enriched in chalcophile components. The absence of sulphides in the lavas could be explained by degassing, but it might be expected that degassed, sulphide-enriched lavas would still be enriched in PGE. A possible explanation, and potential test of the hypothesis that vapour–sulphide interactions played a key role in the formation of the orebodies, is that the erupted equivalents to the ore-forming magmas may be represented not in the lavas but in the pyroclastic rocks of the time-equivalent volcanic stratigraphy.

Animations of 3D microCT scans

Supplementary Data File Norilsk-VZU3-globules.mov (supplementary data are available for downloading at http://www.petrology.oxfordjournals.org) is an animation of a 3D microCT scan of sample VZU-3 showing sulphide globules and the enclosing interstitial sulphide network. File Norilsk-NOR1-1-globules.mov is an animation of a ~100 micron resolution medical CT scan of sample Nor1-1 showing globular sulphides only.

ACKNOWLEDGEMENTS

We are grateful to Norilsk Nickel for access to underground mines and the Medvezhy (Bear) Creek open pit, and to the organizers and field trip leaders of the 2014 International Platinum Conference in Russia for organising field visits and for their heroic efforts in enabling us to get samples out of Russia. The synchrotron X-ray fluorescence maps were collected on the X-ray fluorescence microscopy beamline at the Australian Synchrotron, Clayton, Victoria, Australia, operated by ANSTO, and we acknowledge the assistance of Daryl Howard and David Paterson in data collection. We thank Nadya Krivolutskaya, Marina Yudovskaya, Nick Arndt, Sergei Sluzhenikyn and Chusi Li for the loan of additional samples. The manuscript was improved by helpful reviews from Dima Kamenetsky, Nick Arndt, Marina Yudovskaya and Editor Jim Mungall.

FUNDING

SJB and MLV acknowledge support from the CSIRO Research Plus office. CML acknowledges support from NSERC Discovery grant # 203171–2012.

SUPPLEMENTARY DATA

Supplementary data are available at *Journal of Petrology* online.

REFERENCES

Afonso, J. C., Ranalli, G. & Fernandez, M. (2005). Thermal expansivity and elastic properties of the lithospheric mantle; results from mineral physics of composites. *Physics of the Earth and Planetary Interiors* **149**, 279–306.

Anderson, A. T., Swihart, G. H., Artioli, G. & Geiger, C. A. (1984). Segregation vesicles, gas filter-pressing, and igneous differentiation. *Journal of Geology* **92**, 55–72.

Arndt, N. T. (2011). Insights into the geologic setting and origin of Ni-Cu-PGE sulfide deposits of the Norilsk-Talnakh region, Siberia. *Reviews in Economic Geology* **17**, 199–215.

Arndt, N. T., Czamanske, G. K., Walker, R. J., Chauvel, C. & Fedorenko, V. A. (2003). Geochemistry and origin of the intrusive hosts of the Noril'sk-Talnakh Cu-Ni-PGE sulfide deposits. *Economic Geology and the Bulletin of the Society of Economic Geologists* **98**, 495–515.

Barnes, S. J., Cox, R. A. & Zientek, M. L. (2006). Platinum-group element, gold, silver and base metal distribution in compositionally zoned sulfide droplets from the Medvezky Creek Mine, Noril'sk, Russia. *Contributions to Mineralogy and Petrology* **152**, 187–200.

Barnes, S. J. (1998). Chromite in Komatiites, 1. Magmatic controls on crystallization and composition. *Journal of Petrology* **39**, 1689–1720.

Barnes, S. J., Beresford, S. W. & Le Vaillant, M. (2016a). Interspinifex Ni sulfide ore from the Coronet Shoot, Kambalda: characterisation using microbeam XRF mapping and 3D X-ray computed tomography. *Economic Geology* **111**, 1509–1517.

Barnes, S. J., Cruden, A. R., Arndt, N. T. & Saumur, B. M. (2016b). The mineral system approach applied to magmatic Ni-Cu-PGE sulphide deposits. *Ore Geology Reviews* **76**, 296–316.

Barnes, S. J., Mole, D. R., Le Vaillant, M., Campbell, M., Verrall, M., Roberts, M. & Evans, N. J. (2016c). Poikilitic textures, heteradcumulates and zoned orthopyroxenes in the Ntaka Ultramafic Complex, Tanzania: implications for crystallization mechanisms of oikocrysts. *Journal of Petrology* **57**, 1171–1198.

Barnes, S. J. & Hill, R. E. T. (1995). Poikilitic chromite in komatiitic cumulates. *Mineralogy and Petrology* **54**, 85–92.

Barnes, S. J., Le Vaillant, M. & Lightfoot, P. C. (2017a). Textural development in sulfide-matrix ore breccias and associated rocks in the Voisey's Bay Ni-Cu-Co deposit, Labrador, Canada. *Ore Geology Reviews* **90**, 414–438.

Barnes, S. J., Mungall, J. E., Le Vaillant, M., Godel, B., Lesher, C. M., Holwell, D. A., Lightfoot, P. C., Krivolutskaya, N. A. & Wei, B. (2017b). Sulfide-silicate textures in magmatic Ni-Cu-PGE sulfide ore deposits: disseminated and net-textured ores. *American Mineralogist* **102**, 473–506.

Barnes, S. J. & Robertson, J. C. (2018). Time scales and length scales in magma flow pathways and the origin of magmatic Ni-Cu-PGE ore deposits. *Geoscience Frontiers* **10**, 77–87.

Barnes, S. J., Wells, M. A. & Verrall, M. R. (2009). Effects of magmatic processes, serpentinization and talc carbonate alteration on sulfide mineralogy and ore textures in the Black Swan disseminated nickel sulfide deposit, Yilgarn Craton. *Economic Geology* **104**, 539–562.

Beresford, S. W., Cas, R. A. F., Lambert, D. D. & Stone, W. E. (2000). Vesicles in thick komatiite lava flows, Kambalda, Western Australia. *Journal of the Geological Society* **157**, 11–14.

Brugmann, G. E., Naldrett, A. J., Asif, M., Lightfoot, P. C., Gorbachev, N. S. & Fedorenko, V. A. (1993). Siderophile and chalcophile metals as tracers of the evolution of the Siberian Trap in the Noril'sk region, Russia. *Geochimica et Cosmochimica Acta* **57**, 2001–2018.

Burgess, S. & Bowring, S. (2015). High-precision geochronology confirms voluminous magmatism before, during, and after Earth's most severe extinction. *Science Advances* **1**, e1500470.

Campbell, I. H. (1968). The origin of heteradcumulate and adcumulate textures in the Jimberlana Norite. *Geological Magazine* **105**, 378–383.

Campbell, I. H. (1978). Some problems with the cumulus theory. *Lithos* **11**, 311–323.

Chung, H.-Y. & Mungall, J. E. (2009). Physical constraints on the migration of immiscible fluids through partially molten silicates, with special reference to magmatic sulfide ores. *Earth and Planetary Science Letters* **286**, 14–22.

Czamanske, G. K., Kunilov, V. E., Zientek, M. L., Cabri, L. J., Likhachev, A. P., Calk, L. C. & Oscarson, R. L. (1992). A proton-microprobe study of magmatic sulfide ores from the Noril'sk-Talnakh district, Siberia. *Canadian Mineralogist* **30**, 249–287.

Czamanske, G. K., Zen'ko, K. E., Fedorenko, V., Calk, L. C., Budahn, J. R., Bullock, J. H. J., Fries, T. L., King, B. S. & Siems, D. F. (1995). Petrographic and geochemical characterization of ore-bearing intrusions of the Noril'sk Type, Siberia; with discussion of their origin. *Resource Geology Special Issue* **18**, 1–48.

Distler, V. V., Grokhovskaya, T. L., Evstigneeva, T. L., Sluzheninkin, S. F., Filimonova, A. A. & Dyuzhikov, O. A. (1988). *Petrology of Magmatic Sulfide Ore Mineralization*. Moscow: Naukapp.

Distler, V. V., Kulagov, E. A., Sluzhenikin, S. F. & Laputina, I. P. (1996). Quenched sulphide solutions in Noril'sk ores. *Geology of Ore Deposits* **38**, 41–53.

Distler, V. V., Sluzhenikin, S. F., Cabri, L. J., Krivolutskaya, N. A., Turovtsev, D. M., Golovanova, T. A., Mokhov, A. V., Knauf, V. V. & Oleshkevich, O. I. (1999). Platinum ores of the Noril'sk layered intrusions: magmatic and fluid concentration of noble metals. *Geology of Ore Deposits* **41**, 214–237.

Donaldson, C. H., Drever, H. I. & Johnston, R. (1973). Crystallization of poikilo-macrospherulitic feldspar in a Rhum peridotite. *Nature Physical Science* **243**, 69–70.

Dyuzhikov, O. A., Distler, V. V., Strunin, B. M., Cherman, M. L. & Sluzhenikin, S. F. (1988). Copper-nickel sulfide ore-bearing formations. In: Duzhikov, O. A. & Distler, V. V. (eds) *Geology and Metallogeny of Sulfide Deposits, Noril'sk Region USSR, Special Publication No. 1*. Littleton: Society of Economic Geologists, pp. 61–146.

Eckstrand, R. O. & Williamson, B. L. (1985). Vesicles in the Dundonald komatiites. *Program and Abstracts, Geological Association of Canada—Mineralogical Association of Canada Annual Meeting* **10**, A-16.

Fedorenko, V. A. (1994). Evolution of magmatism as reflected in the volcanic sequence of the Noril'sk region. In: Lightfoot, P. C. & Naldrett, A. J. (eds) *Proceedings of the Sudbury-Noril'sk Symposium, Ontario Geological Survey Special Publication 5*. Toronto: Ontario Geological Survey, pp. 171–184.

Genkin, A. D., Distler, V. V., Gladyshev, G. D., Filimonova, A. A., Evstigneeva, T. L., Kovalenker, V. A., Laputina, I. P., Smirnov, A. V. & Grokhovskaya, T. L. (1982). *Sulfide Copper-nickel Ores of the Noril'sk Deposits*. Moscow: Nauka, pp. 234.

Godel, B. (2013). High-resolution X-ray computed tomography and its application to ore deposits: from data acquisition to quantitative three-dimensional measurements with case studies from Ni-Cu-PGE deposits. *Economic Geology* **108**, 2005–2019.

Godel, B., Barnes, S. J. & Barnes, S.-J. (2013). Deposition mechanisms of magmatic sulphide liquids: evidence from

high-resolution X-ray computed tomography and trace element chemistry of komatiite-hosted disseminated sulphides. *Journal of Petrology* **54**, 1455–1481.

Godel, B., Ellis, B., O'Dea, D., Honeyands, T. & Harvey, T. (2017). Digital rocks for iron ore sinters—toward a 3D quantification of sinter textures. *Proceeding of Iron Ore 2017 Conference*. Perth: Australasian Institute of Mining and Metallurgy, pp. 529–534.

Godel, B. M., Barnes, S. J., Gurer, D., Austin, P. & Fiorentini, M. L. (2013). Chromite in komatiites: 3D morphologies with implications for crystallization mechanisms. *Contributions to Mineralogy and Petrology* **165**, 173–189.

Godlevsky, M. N. (1959). *Traps and Ore-bearing Intrusions of the Noril'sk Region*. Moscow: Gosgeoltekhizdat, pp. 69.

Higgins, M. D. (1998). Origin of anorthosite by textural coarsening; quantitative measurements of a natural sequence of textural development. *Journal of Petrology* **39**, 1307–1323.

Hill, R. E. T. (1984). Experimental study of phase relations at 600°C in a portion of the Fe-Ni-Cu-S system and its application to natural sulphide assemblages. In: Buchanan, D. L. & Jones, M. J. (eds) *Sulphide Deposits in Mafic and Ultramafic Rocks*. London: Institute of Mining and Metallurgy, pp. 14–21.

Hill, R. E. T., Barnes, S. J., Dowling, S. E. & Thordarson, T. (2004). Komatiites and nickel sulfide ores of the Black Swan area, Yilgarn Craton, Western Australia. 1. Petrology and volcanology of host rocks. *Mineralium Deposita* **39**, 684–706.

Holwell, D. A., Abraham-James, T., Keays, R. R. & Boyce, A. J. (2012). The nature and genesis of marginal Cu-PGE-Au sulphide mineralisation in Paleogene Macrodykes of the Kangerlussuaq region, East Greenland. *Mineralium Deposita* **47**, 3–21.

Holwell, D. A., Adeyemi, Z., Ward, L. A., Smith, D. J., Graham, S. D., McDonald, I. & Smith, J. W. (2017). Low temperature alteration of magmatic Ni-Cu-PGE sulfides as a source for hydrothermal Ni and PGE ores: a quantitative approach using automated mineralogy. *Ore Geology Reviews* **91**, 718–740.

Iacono-Marziano, G., Ferraina, C., Gaillard, F., Di Carlo, I. & Arndt, N. T. (2017). Assimilation of sulfate and carbonaceous rocks: experimental study, thermodynamic modeling and application to the Noril'sk-Talnakh region (Russia). *Ore Geology Reviews* **90**, 399–413.

Iacono-Marziano, G., Marecal, V., Pirre, M., Gaillard, F., Arteta, J., Scaillet, B. & Arndt, N. T. (2012). Gas emissions due to magma-sediment interactions during flood magmatism at the Siberian Traps; gas dispersion and environmental consequences. *Earth and Planetary Science Letters* **357-358**, 308–318.

Keele, R. A. & Nickel, E. H. (1974). The geology of a primary millerite-bearing sulfide assemblage and supergene alteration at the Otter Shoot, Kambalda, Western Australia. *Economic Geology* **69**, 1102–1117.

Kirkham, R., Dunn, P., Kuczewski, A., Siddons, D., Dodanwela, R., Moorhead, G., Ryan, C.D., Geronimo, G., Beuttenmuller, R., Pinelli, D., Pfeffer, M., Davey, P., Jensen, M., Paterson, D., de Jonge, M., Kusel, M. & McKinlay, J. (2010). The Maia spectroscopy detector system: engineering for integrated pulse capture, low-latency scanning and real-time processing. *Proceedings of Australian Institute of Physics* **1234**, 240–243.

Kotulskii, V. K. (1946). Genesis of magmatic Cu-Ni deposits. *Doklady Akadamia Nauk SSSR* **51**, 381–384.

Kress, V., Greene, L. E., Ortiz, M. D. & Mioduszewski, L. (2008). Thermochemistry of sulfide liquids IV; density measurements and the thermodynamics of O-S-Fe-Ni-Cu liquids at low to moderate pressures. *Contributions to Mineralogy and Petrology* **156**, 785–797.

Krivolutskaya, N. A. (2014). *Evolution of Trap Magmatism and Processes Producing Pt-Cu-Ni Mineralization in the Noril'sk Area (in Russian)*. Moscow: KMK.

Krivolutskaya, N. A. (2011). Formation of PGM–Cu–Ni deposits in the process of evolution of flood basalt magmatism in the Noril'sk region. *Geology of Ore Deposits* **53**, 309–339.

Krivolutskaya, N. A., Ariskin, A. A., Sluzhenikin, S. F. & Turovtsev, D. M. (2001). Geochemical thermometry of rocks of the Talnakh intrusion: assessment of the melt composition and the crystallinity of the parental magma. *Petrology* **9**, 389–414.

Krivolutskaya, N., Tolstykh, N., Kedrovskaya, T., Naumov, K., Kubrakova, I., Tyutyunnik, O., Gongalsky, B., Kovalchuk, E., Magazina, L., Bychkova, Y. & Yakushev, A. (2018a). World-class PGE-Cu-Ni Talnakh deposit: new data on the structure and unique mineralization of the south-western branch. *Minerals* **8**, 124.

Krivolutskaya, N. A., Gongalsky, B. I., Kedrovskaya, T. B., Kubrakova, I. V., Tyutyunnik, O. A., Chikatueva, V. Y., Bychkova, Y. V., Magazina, L., Kovalchuk, E. N., Yakushev, A. I. & Kononkova, N. N. (2018b). Geology of the western flanks of the Oktyabr'skoe deposit, Noril'sk district, Russia: evidence of a closed magmatic system. *Mineralium Deposita* in press (online), doi: 10.1007/s00126-018-0827-z.

Kullerud, G., Yund, R. A. & Moh, G. H. (1969). Phase relations in the Cu-Fe-S, Cu-Ni-S and Fe-Ni-S systems. In: Wilson, H. D. B. (ed.) *Magmatic Ore Deposits, Economic Geology Monograph* **4**, pp. 323–343. Society of Economic Geologists.

Latypov, R. M. (2002). Phase equilibria constraints on relations of ore-bearing intrusions with flood basalts in the Noril'sk region, Russia. *Contributions to Mineralogy and Petrology* **143**, 438–449.

Le Vaillant, M., Barnes, S. J., Mungall, J. E. & Mungall, E. (2017). Role of de-gassing of the Noril'sk nickel deposits in the Permo-Triassic mass extinction event. *Proceedings of the National Academy of Sciences* **114**, 2485–2490.

Lesher, C. M. (2017). Roles of residues/skarns, xenoliths, xenocrysts, xenomelts, and xenovolatiles in the genesis, transport, and localization of magmatic Fe-Ni-Cu-PGE sulfides and chromite. *Ore Geology Reviews* **90**, 465–484.

Li, C., Ripley, E. M., Naldrett, A. J., Schmitt, A. K. & Moore, C. H. (2009). Magmatic anhydrite-sulfide assemblages in the plumbing system of the Siberian Traps. *Geology* **37**, 259–262.

Lightfoot, P. C. & Naldrett, A. J. (1984). Chemical variation in the Insizwa Complex, Transkei, and the nature of the parent magma. *Canadian Mineralogist* **22**, 111–123.

Lightfoot, P. C. & Zotov, I. A. (2014). Geological relationships between the intrusions, country rocks and Ni-Cu-PGE sulfides of the Kharealakh Intrusion, Noril'sk region: implications for the role of sulfide differentiation and metasomatism in their genesis. *Northwestern Geology* **47**, 1–35.

Likhachev, A. P. (1994). Ore-bearing intrusions of the Noril'sk region. In: Lightfoot, P. C. & Naldrett, A. J. (eds) *Proceedings of the Sudbury-Noril'sk Symposium. Ontario Geological Survey Special Publication 5*. Toronto, ON: Ontario Geological Survey, pp. 185–201.

Magee, C., O'Driscoll, B., Petronis, M. S. & Stevenson, C. T. E. (2016a). Three-dimensional magma flow dynamics within subvolcanic sheet intrusions. *Geosphere* **12**, 842–866.

Magee, C., Muirhead, J. D., Karvelas, A., Holford, S. P., Jackson, C. A. L., Bastow, I. D., Schofield, N., Stevenson, C. T. E.,

McLean, C., McCarthy, W. & Shtukert, O. (2016b). Lateral magma flow in mafic sill complexes. *Geosphere* **12**, 809–841.

Malitch, K. N., Latypov, R. M., Badanina, I. Y. & Sluzhenikin, S. F. (2014). Insights into ore genesis of Ni-Cu-PGE sulfide deposits of the Noril'sk Province (Russia); evidence from copper and sulfur isotopes. *Lithos (Oslo)* **204**, 172–187.

Martin, E. & Sigmarsson, O. (2007). Low pressure differentiation of tholeiitic lavas as recorded in segregation veins from Reykjanes (Iceland), Lanzarote (Canary Islands) and Masaya (Nicaragua). *Contributions to Mineralogy and Petrology* **154**, 559–573.

Mathison, C. I. (1987). Pyroxene oikocrysts in troctolitic cumulates; evidence for supercooled crystallization and postcumulus modification. *Contributions to Mineralogy and Petrology* **97**, 228.

McBirney, A. R. & Hunter, R. H. (1995). The cumulate paradigm reconsidered. *Journal of Geology* **103**, 114–122.

McBirney, A. R. & Noyes, R. M. (1979). Crystallization and layering in the Skaergaard Intrusion. *Journal of Petrology* **20**, 487–554.

Merle, R., Caroff, M., Girardeau, J., Cotten, J. & Guivel, C. (2005). Segregation vesicles, cylinders, and sheets in vapor-differentiated pillow lavas: examples from Tore-Madeira Rise and Chile Triple Junction. *Journal of Volcanology and Geothermal Research* **141**, 109–122.

Mungall, J. E. (2002). Late-stage sulfide liquid mobility in the main mass of the Sudbury Igneous Complex: examples from the Victor Deep, McCreedy East, and Trillabelle deposits. *Economic Geology* **97**, 1563–1576.

Mungall, J. E. (2007). Crystallization of magmatic sulfides; an empirical model and application to Sudbury ores. *Geochimica et Cosmochimica Acta* **71**, 2809.

Mungall, J. E. (2015). Physical controls of nucleation, growth and migration of vapor bubbles in partially molten cumulates. In: Charlier, B., Namur, O., Latypov, R., Tegner, C. (eds) *Layered Intrusions*. Heidelberg: Springer, pp. 331–378.

Mungall, J. E., Brenan, J. M., Godel, B., Barnes, S. J. & Gaillard, F. (2015). Transport of S, Cu and Au in magmas by flotation of sulphide melt on vapour bubbles. *Nature Geoscience* **8**, 216–219.

Naldrett, A. J. (1989). Ores associated with flood basalts. *Reviews in Economic Geology* **4**, 103.

Naldrett, A. J. (1999). World-class Ni-Cu-PGE deposits: key factors in their genesis. *Mineralium Deposita* **34**, 227–240.

Naldrett, A. J. (2004). *Magmatic Sulfide Deposits: Geology, Geochemistry and Exploration*. Heidelberg: Springer, pp. 727.

Naldrett, A. J. & Lightfoot, P. C. (1999). Ni-Cu-PGE deposits of the Noril'sk region, Siberia: their formation in conduits for flood basalt Volcanism. In: Keays, R. R., Lesher, C. M., Lightfoot, P. C., Farrow, C. E. G. (eds). Sudbury: Geological Association of Canada Short Course 13, pp. 195–249.

Naldrett, A. J., Lightfoot, P. C., Fedorenko, V., Doherty, W. & Gorbachev, N. S. (1992). Geology and geochemistry of intrusions and flood basalts of the Noril'sk region, USSR, with implications for the origin of the Ni-Cu ores. *Economic Geology* **87**, 975–1004.

Natorkhin, I. A., Arkhipova, A. I. & Batuev, B. N. (1977). *Petrology of the Talnakh Intrusions*. Leningrad: Nedrapp.

Paterson, D. D., Jonge, M. D., Howard, D. L., Lewis, W., McKinlay, J., Starritt, A., Kusel, M., Ryan, C. G., Kirkham, R., Moorhead, G. & Siddons, D. P. (2011). The X-ray fluorescence microscopy beamline at the Australian synchrotron. *Proceedings of the Australian Institute of Physics* **1365**, 219–222.

Prichard, H. M., Hutchinson, D. & Fisher, P. C. (2004). Petrology and crystallization history of multiphase sulfide droplets in a mafic dike from Uruguay: implications for the origin of Cu-Ni-Pge sulfide deposits. *Economic Geology and the Bulletin of the Society of Economic Geologists* **99**, 365–376.

Rampino, M. R., Rodriguez, S., Baransky, E. & Cai, Y. (2017). Global nickel anomaly links Siberian Traps eruptions and the latest Permian mass extinction. *Nature Scientific Reports* **7**, 12416.

Ripley, E. M., Lightfoot, P. C., Li, C. & Elswick, E. R. (2003). Sulfur isotopic studies of continental flood basalts in the Noril'sk region: implications for the association between lavas and ore-bearing intrusions. *Geochimica et Cosmochimica Acta* **67**, 2805–2817.

Robertson, J. C., Barnes, S. J. & Le Vaillant, M. (2015). Dynamics of magmatic sulphide droplets during transport in silicate melts and implications for magmatic sulphide ore formation. *Journal of Petrology* **56**, 2445–2472.

Rothman, D. H., Fournier, G. P., French, K. L., Alm, E. J., Boyle, E. A., Cao, C. & Summons, R. E. (2014). Methanogenic burst in the end-Permian carbon cycle. *Proceedings of the National Academy of Sciences* **111**, 5462–5467.

Ryabov, V. V., Shevko, A. Y. & Gora, M. P. (2014). *Trap Magmatism and Ore Formation in the Siberian Noril'sk Region*. Dordrecht: Springer, pp.625.

Ryan, C. G., Siddons, D. P., Kirkham, R., Li, Z. Y., de Jonge, M. D., Paterson, D. J., Kuczewski, A., Howard, D. L., Dunn, P. A., Falkenberg, G., Boesenberg, U., De Geronimo, G., Fisher, L. A., Halfpenny, A., Lintern, M.J.., Lombi, E., Dyl, K. A., Jensen, M., Moorhead, G. F., Cleverley, J. S., Hough, R. M., Godel, B., Barnes, S. J., James, S. A., Spiers, K. M., Alfeld, M., Wellenreuther, G., Vukmanovic, Z. & Borg, S. (2014). Maia X-ray fluorescence imaging: capturing detail in complex natural samples. *Journal of Physics: Conference Series* **499**, 012002.

Sanders, I. S. (1986). Gas filter-pressing origin for segregation vesicles in dykes. *Geological Magazine* **123**, 67–72.

Siégel, C., Arndt, N. T., Barnes, S.J., Henriot, A.-L., Haenecour, P., Debaille, V. & Mattielli, N. (2014). Fred's Flow (Canada) and Murphy Well (Australia): thick komatiitic lava flows with contrasting compositions, emplacement mechanisms and water contents. *Contributions to Mineralogy and Petrology* **168**, 1084.

Sigmarsson, O., Thordarson, T. & Jakobsson, S. P. (2009). Segregations in Surtsey lavas (Iceland) reveal extreme magma differentiation during late stage flow emplacement. *Special Publications of the International Association of Volcanology and Chemistry of the Earth's Interior* **2**, 85–104.

Sluzhenikin, S., Distler, V., Dyuzhikov, O., Kravtsov, V., Kunilov, V., Laputina, I. & Turovtsev, D. (1994). Low sulphide platinum mineralization of the Noril'sk differentiated intrusions. *Geology of Ore Deposits* **36**, 171–195.

Sluzhenikin, S. F., Krivolutskaya, N. A., Rad'ko, V., Malitch, K. N., Distler, V. V. & Fedorenko, V. A. (2014). *Ultramafic-mafic Intrusions, Volcanic Rocks and PGE-Cu-Ni Sulfide Deposits of the Noril'sk Province, Polar Siberia, Field Trip Guidebook*. Yekaterinburg, Russia: Institute of Geology of Ore Deposits, Petrography, Mineralogy and Geochemistry.

Smith, R. E. (1967). Segregation vesicles in basaltic lava. *American Journal of Science* **265**, 696–713.

Spiridonov, E. M. (2010). Ore-magmatic systems of the Noril'sk ore field. *Russian Geology and Geophysics* **51**, 1059–1077.

Stone, W. E., Crocket, J. H. & Fleet, M. E. (1996). Platinum-group mineral occurrence associated with flow top amygdule sulfides in komatiitic basalt, Abitibi Greenstone Belt, Ontario. *Mineralogy and Petrology* **56**, 1–24.

Tegner, C. & Wilson, J. R. (1995). Textures in a poikilitic olivine gabbro cumulate; evidence for supercooling. *Mineralogy and Petrology* **54**, 161–173.

Tenailleau, C., Etschmann, B., Wang, H., Pring, A., Grguric, B. A. & Studer, A. (2005). Thermal expansion of troilite and pyrrhotite determined by in situ cooling (873 to 373 K) neutron powder diffraction measurements. *Mineralogical Magazine* **69**, 205–216.

Urvantsev, N. N. (1972). Some aspects of formation of Norilsk ore-bearing intrusions and ores. *Copper-nickel Ores of the Talnakh Ore Junction*. Leningrad, pp. 100–105.

Wager, L. R. & Brown, G. M. (eds) (1968). *Layered Igneous Rocks*. Edinburgh and London: Oliver and Boyd.

Wager, L. R., Brown, G. M. & Wadsworth, W. J. (1960). Types of igneous cumulates. *Journal of Petrology* **1**, 73–85.